FOUNDATIONS FOR ECOLOGICAL RESEARCH WEST OF THE ANTARCTIC PENINSULA
ANTARCTIC RESEARCH SERIES, VOLUME 70, PAGES 81-104

SPATIAL AND TEMPORAL VARIABILITY OF WESTERN ANTARCTIC PENINSULA SEA ICE COVERAGE

S. E. Stammerjohn and R. C. Smith

Institute for Computational Earth System Science (ICESS), Geography Department, University of California, Santa Barbara

Spatial and temporal variability of sea ice coverage west of the Antarctic Peninsula, the Palmer Long Term Ecological Research (LTER) study area, is analyzed from October 1978 to August 1994, using surface sea ice concentrations derived from passive microwave satellite data. Ice coverage in the LTER region, nearby regions and the Southern Ocean are compared. Results show that various regions have distinct characteristics in seasonal and interannual variability in contrast to the Southern Ocean as a whole. For example, *seasonal* ice coverage in the LTER and Bellingshausen regions is distinct from other Southern Ocean regions in that the period of ice advance is relatively short in comparison to the period of ice retreat. In addition, the LTER and Bellingshausen regions are the only Southern Ocean regions which show long term persistence in monthly anomalous ice coverage, so that there is an oscillation between several consecutive high ice years followed by several consecutive low ice years. Cross spectral analysis of monthly anomalous ice coverage was performed to determine the longitudinal spatial extent of coherence among regions. There is no coherence between the eastern Antarctic Peninsula and LTER regions. There is low frequency coherence between Bellingshausen and Amundsen monthly anomalies, and the phase indicates that anomalous ice coverage in the Bellingshausen lags the Amundsen by approximately one year. Within the Bellingshausen region there is both high and low frequency coherence and a west-to-east propagation of anomalies. Comparisons of ice concentrations calculated from passive microwave and visible satellite data show that passive microwave derived ice concentrations overestimate surface ice concentrations between 0-40% (17.4% ±17.8%) and 40-75% (10.8% ±11.3%) but underestimate surface ice concentrations between 75-100% (9.2% ±6.9%). Ecological implications, as revealed by both the low and high resolution satellite data, are discussed. This LTER sea ice record provides a basis against which life-history parameters of primary producers and populations of key species from different trophic levels can be monitored and against which oceanographic and atmospheric variability in this region can be compared and modeled.

1. INTRODUCTION

A dominant and distinguishing characteristic of Southern Ocean marine ecology is sea ice, which ranges from a minimum extent of 4 x 10^6 km^2 in February to a maximum extent of about 20 x 10^6 km^2 in September [*Gordon and Taylor,* 1975; *Zwally et al.*, 1983], defining a seasonal sea ice zone which is more than the area of the Antarctic continent itself (13.2 x 10^6 km^2). Sea ice and the overlying snow cover influence ocean-atmosphere exchanges by modifying albedo, heat exchanges, momentum transfers and oceanic salt flux. The presence of an ice/snow cover changes the input of solar radiation to the water column, affecting marine biological processes and the heat balance of the upper ocean. The freezing and melting of sea ice contribute to the variability in salinity, and hence density gradients, of the upper ocean, thus influencing the vertical structure of phytoplankton distributions and abundances. From an ecological perspective, sea ice is a habitat, feeding site, refuge and breeding ground for organisms at all trophic levels. The marginal ice zone (MIZ), delimited by the influence of low density meltwater and scattered ice flows from the receding pack ice and by the penetration of ocean swell into the pack ice, is an ecosystem boundary where the flow of energy, the cycling of chemical elements and biological communities change dramatically. Often the MIZ is also an area of high biological productivity [*Smith and Nelson,* 1985; *Wilson et al.*, 1986; *Nelson et al.*, 1987; *Dieckmann,* 1987; *Sullivan et al.*, 1988; *Nelson et al.*, 1989; *Smith and Nelson,* 1990; *Comiso et al.*, 1990; *Comiso et al.*, 1993]. Thus, sea ice is a key environmental variable of the Southern Ocean, and quantification of sea ice parameters, such as concentration, extent, thickness and timing of autumn advance and spring retreat, is essential to understanding linkages between sea ice and the Southern Ocean marine ecosystem.

A central hypothesis of the Palmer Long-Term Ecological Research (LTER) program [*Quetin and Ross,* 1992; *Ross and Quetin,* 1992], based at Palmer Station on the southwest side of Anvers Island (Figure 1), is that biological processes in the Antarctic marine environment are strongly affected by physical factors, in particular the annual advance and retreat of pack ice. Interannual cycles and/or trends in annual pack ice are hypothesized to have significant effects on all levels of the food web, from total annual primary production to breeding success in seabirds [*Ainley et al.*, 1986; *Fraser and Ainley,* 1986; *Smith and Vidal,* 1986; *Smith and Nelson,* 1986; *Walsh and McRoy,* 1986; *Garrison et al.*, 1987; *Ainley et al.*, 1988]. In addition to the direct ecological consequences, variability in sea ice coverage is a critical element in the complex atmo-

sphere-hydrosphere-cryosphere global climate system. Ice-atmosphere [*Streten and Pike*, 1980; *Carleton*, 1981; *Cavalieri and Parkinson*, 1981; *Budd*, 1982; *Parkinson and Cavalieri*, 1982; *Zwally et al.*, 1983; *Carleton and Carpenter*, 1989] and ice-oceanic [*Gordon and Taylor*, 1975; *Gordon*, 1981; *Hibler and Ackley*, 1983] coupling have been demonstrated at various strengths and over a wide range of spatial and temporal scales. In addition, variability in sea ice may be a possible indicator of long-term climate change [*Cavalieri and Zwally*, 1985; *Mitchell*, 1989; *Manabe et al.*, 1991; *Manabe et al.*, 1992]. As a consequence of its central ecological importance, sea ice may play a key role in coupling physical and biological processes on shorter time scales to longer term processes.

In the following we document the interannual and annual variability in western Antarctic Peninsula sea ice coverage from October 1978 to August 1994, with particular emphasis on the LTER study area. We make use of satellite data, both low resolution passive microwave and high resolution visible and infrared data, to investigate spatial and temporal variability of sea ice and the marine ecological significance of this variability. In addition, we directly compare the low and high resolution sea ice estimates and discuss the ecological implications of the low versus high resolution perspective. In Section 2 we provide a brief background for the remote sensing of sea ice, and in Section 3 we give a discussion and evaluation of sea ice concentration algorithms. In Section 4 the methodology for sea ice data analysis is described, and results are presented in Section 5. Discussion and summary are given in Section 6.

2. SATELLITE IMAGERY

2.1. Passive Microwave Data

Passive microwave remote sensing of the Southern Ocean provides the most complete temporal record of the annual advance and retreat of Antarctic sea ice, because it is not limited by clouds or polar darkness. However, a disadvantage of these passive microwave data is the spatial resolution which is on the order of tens of kilometers. The passive microwave data used in this study were provided by the National Snow and Ice Data Center (NSIDC) which distributes data from NASA's Scanning Multi-Channel Microwave Radiometer (SMMR) and from the Defense Meteorological Satellite Program's (DMSP) Special Sensor Microwave/Imager (SSM/I). SMMR was in operation from October 1978 to August 1987, and SSM/I has been in operation since July 1987. The SMMR sensor was carried onboard a sun-synchronous near-polar orbiting satellite, as is the SSM/I sensor, however SMMR operated on alternate days, while SSM/I is in continuous operation, providing two to three daily passes of polar regions. SMMR was dual polarized at five frequencies (6.63, 10.69, 18.0, 21.0 and 37.0 GHz), and SSM/I at three frequencies (19.35, 37.0, and 85.5 GHz) and vertically polarized at 22.235 GHz. The 18.0 GHz (or 19.35 GHz) and 37.0 GHz channels are typically used in most sea ice algorithms. The effective field of view or spatial resolution at these frequencies range from 69 by 43 km at SSM/I 19.35 GHz (or from 54 by 35 km at SMMR 18.0 GHz) to 37 by 28 km at SSM/I 37.0 GHz (or 28 by 18 km at SMMR 37.0 GHz). Detailed SMMR sensor description and operating characteristics are provided by *Gloersen and Barath* [1977]. *Hollinger et al.* [1987] provide similar information on the SSM/I sensor.

The NSIDC SMMR and SSM/I archive from October 1978 to August 1994 contains both brightness temperatures and derived ice concentrations. Both SMMR and SSM/I derived ice concentrations are binned to 25 km square cells in a polar stereographic projection. The ice concentration grids for the Southern Ocean include coverage from 50° to 87°S. The archive also contains a landmask and latitude and longitude pairs for geolocating pixels.

2.2. Visible and Infrared Data

The Advanced Very High Resolution Radiometer (AVHRR) was first launched on the Television Infrared Observational Satellite (TIROS-N) in 1978 and is currently carried on the National Oceanic and Atmospheric Administration (NOAA) weather satellites. AVHRR was primarily built for meteorological studies. The very high resolution referred to in its acronym comes from an improved radiometric resolution at 10-bit or 1024 gray levels [*Pease*, 1991]. The spatial resolution is approximately 1.1 km at nadir. There are two satellites in sun-synchronous near-polar orbits at an altitude of 850 km. Each satellite orbits the earth 14 times a day, crossing the equator at 0730/1930 and 0200/1400 local sun times, respectively. Complete global coverage is obtained every 24 hours. The near-polar orbit offers good temporal coverage of polar regions, so that at latitudes 60° and above, the distance between ground tracks is less than half the swath width, allowing a point on the surface to be monitored on two to three consecutive passes twice a day.

The AVHRR/2 instrument, first launched in June 1981, has five channels, as opposed to four on the original AVHRR instrument. These channels range from visible to thermal infrared frequencies: (1) 0.58-0.68 mm (red), (2) 0.725-1.10 mm (near-infrared), (3) 3.55-3.93 mm (middle infrared), (4) 10.50-11.50 mm (thermal infrared), and (5) 11.50-12.50 mm (thermal infrared). The time period, September to December 1991, was selected for the high versus low resolution comparison, because we had coincident SSM/I and AVHRR data for this time period, and because the LTER field season began in the austral spring of 1991. AVHRR/2 High Resolution Picture Transmission (HRPT) telemetry from NOAA-10 and NOAA-11 satellites were collected at Palmer Station, Anvers Island and archived by the Arctic and Antarctic Research Center (AARC) at Scripps Institution of Oceanography. Because there are two to four passes available for each day, there were 350 images for the four month period from which cloud-free imagery of the western Antarctic Peninsula region were selected.

3. SEA ICE CONCENTRATION ALGORITHMS

3.1. Passive Microwave NASA Team Algorithm

There are several sea ice concentration algorithms that can be used with SMMR and SSM/I data, and a review of the theory and performance of passive microwave algorithms is given

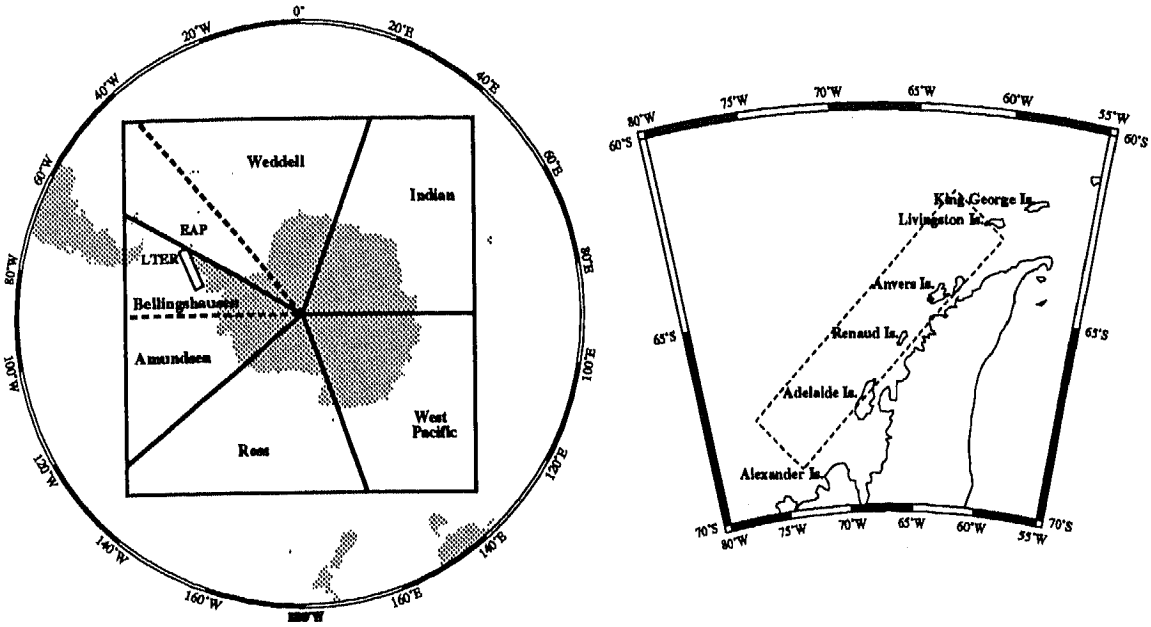

Fig. 1. The Southern Ocean and LTER regional maps in polar stereographic projection. In the Southern Ocean regional map, the large square outlines the NSIDC grid, the heavy lines outline five regions: Weddell (60°W-20°E), Indian (20-90°E), West Pacific (90-160°E), Ross (160°E-130°W) and Amundsen/Bellingshausen (60-130°W), and the dotted lines delineate subregions: the eastern Antarctic Peninsula (EAP, 40-60°W), the Bellingshausen (60-90°W) and the Amundsen (90-130°W). In both maps the rectangle to the west of the Antarctic Peninsula denotes the LTER region.

by *Steffen et al.* [1992]. Two of the most widely used passive microwave ice concentration algorithms are the NASA Team [*Cavalieri et al.*, 1984; *Gloersen and Cavalieri*, 1986] and Goddard Space Flight Center (GSFC) Bootstrap [*Comiso*, 1983; *Comiso et al.*, 1984] algorithms. NSIDC distributes 1987-91 SSM/I ice concentrations derived from both the NASA Team and Bootstrap algorithms, but distributes 1978-87 SMMR and 1992-present SSM/I ice concentrations derived from the NASA Team algorithm only. Because a longer historical record is provided by NSIDC for the NASA Team derived ice concentrations (1978-94), this study will utilize those data.

The NASA Team algorithm was first formalized by *Cavalieri et al.* [1984] to derive sea ice parameters from SMMR data and was later improved by *Gloersen and Cavalieri* [1986] to reduce weather-related effects over open ocean areas. Beginning July 1987 the NASA Team algorithm was applied to SSM/I data, and it was again improved by an additional weather filter based on the 22 GHz channel [*Cavalieri et al.*, 1995]. The NASA Team algorithm utilizes the 18.0 (SMMR) or 19.35 GHz (SSM/I) dual polarized channels and the 37.0 GHz vertically polarized channel to calculate sea ice concentrations. Two ratios, a normalized polarization ratio (PR) and a normalized spectral gradient ratio (GR), are used to classify three surface types: calm open water, first-year sea ice and multiyear sea ice. However, multiyear sea ice in the Southern Ocean is not as well defined radiometrically from first-year sea ice as it is in the Arctic for frequencies less than 40 GHz [*Gow et al.*, 1982]. Therefore, for Southern Ocean applications, the third surface type identified is a second type of first year sea ice. Algorithm tie-points or reference values for the three surface types are empirically determined and used in conjunction with the ratios to determine total sea ice concentrations (and for Arctic applications, first year and multiyear sea ice fractions). The tie-points used in this study are two sets of Southern hemispheric tie-points, one set for the SMMR data [*Gloersen et al.*, 1992] and one set for the SSM/I data [*Cavalieri et al.*, 1991]. Using hemispheric tie points assumes that the brightness temperatures (T_b's) determined for the three surface types (i.e., open water and the two types of first year sea ice) are spatially and temporally consistent throughout the Southern Ocean. *Steffen and Schweiger* [1991] found that using locally/seasonally adjusted tie-points improved algorithm accuracy. However, since locally and seasonally adjusted tie-points are not readily available operationally, we limit our study to the use of the NASA Team algorithm implemented with hemispheric tie points.

Validation of the NASA Team algorithm for Southern Ocean sea ice concentrations is limited, because most validation efforts focus in Arctic regions due to easier logistics (a review of validation efforts is given in *Cavalieri et al.* [1992]). However, there have been two validation studies conducted in Southern Ocean regions which compared SMMR or SSM/I derived ice concentrations using the NASA Team algorithm against other satellite derived ice concentration datasets [*Martin et al.*, 1987; *Steffen and Schweiger*, 1991]. For an October

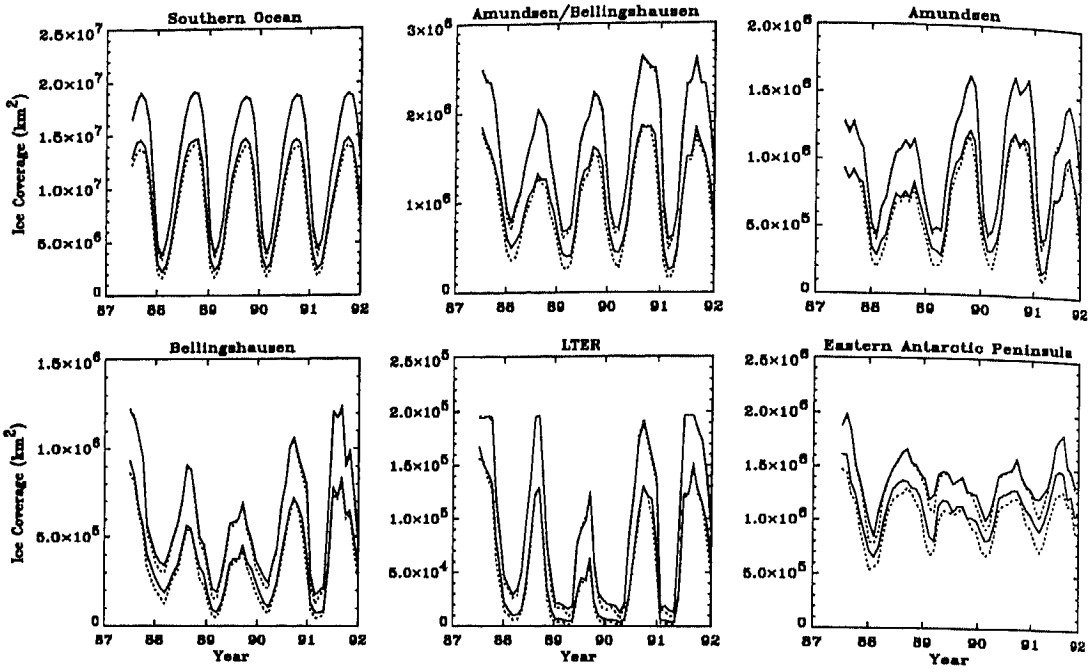

Fig. 2. Monthly ice coverage for selected regions of the Southern Ocean from July 1987 to December 1991. NASA Team and Bootstrap derived ice concentrations are designated by the solid and dotted lines, respectively, and the upper and lower sets of curves denote ice extent and ice coverage, respectively.

Weddell Sea image, which included greater than 40% ice concentrations, *Martin et al.* [1987] found a mean difference of 1.7% ±7.4% between SIR-B and NASA Team SMMR derived ice concentrations. For November Weddell and December Amundsen scenes, which included greater than 70% ice concentrations, *Steffen and Schweiger* [1991] found mean differences of -1.1% ±3.1% and 1.3% ±3.6%, respectively, between Landsat and NASA Team SSM/I derived ice concentrations. Both of these validation studies involved scenes of greater than 40% ice concentrations, and as noted by *Comiso et al.* [1992], the accuracy of ice concentration estimates using the NASA Team or any other similar algorithm will depend on the proportion of new or melting sea ice within the region of study. Because the sea ice ecology of the Palmer LTER region is likely to be significantly influenced by the MIZ, leads and polynyas, one of the objectives of this study is to compare estimates made using the NASA Team algorithm of ice concentrations less than 40% (e.g. MIZ and coastal regions) with estimates made using higher resolution AVHRR imagery.

To determine if there is a bias due to the selection of the NASA Team algorithm over the Bootstrap algorithm, a comparison was made between the NASA Team and Bootstrap derived ice concentrations from July 1987 to December 1991, the period for which NSIDC distributes both sets of ice concentrations. Figure 2 shows the time series of monthly ice concentrations for selected regions of the Southern Ocean (see Figure 1 and Section 4.1 for regional definitions). Two types of ice concentration variables are shown for both the NASA Team and Bootstrap algorithms: ice extent (area inside the 10% ice concentration contour, inclusive of both sea ice and open water) which is denoted by the upper set of curves, and ice coverage (area of sea ice only) which is denoted by the lower set of curves. There is very close agreement between the NASA Team and Bootstrap determinations of ice extent (the curves nearly overlap) except during summer months, where the NASA Team algorithm predicts higher ice extents than the Bootstrap algorithm. However, there are greater discrepancies between the ice coverage curves, where on average the NASA Team algorithm predicts higher ice coverage, especially during maximum and minimum ice coverage.

It is important to note that the comparative agreement between the two algorithms shown in Figure 2 is the result of spatially and temporally averaged data. For daily pixel by pixel comparisons, differences between the two algorithms can be significant. Figure 3 shows a daily pixel by pixel comparison of ice concentrations derived from the two algorithms *for the LTER region only*. February, May, August and November were selected as representative months of summer, fall, winter and spring, respectively, and the end-of-month day was randomly selected to exemplify the daily contrast between the ice concentrations derived from the two algorithms. A complete daily analysis shows that the NASA Team algorithm on average predicts higher ice concentrations both in summer and spring, but in fall and winter, the Bootstrap algorithm predicts higher concentrations at the ice edge and in the interior of the pack ice. However, the higher Bootstrap ice concentrations are often offset by higher NASA Team ice concentrations in areas between the ice edge and the interior pack ice. This offset

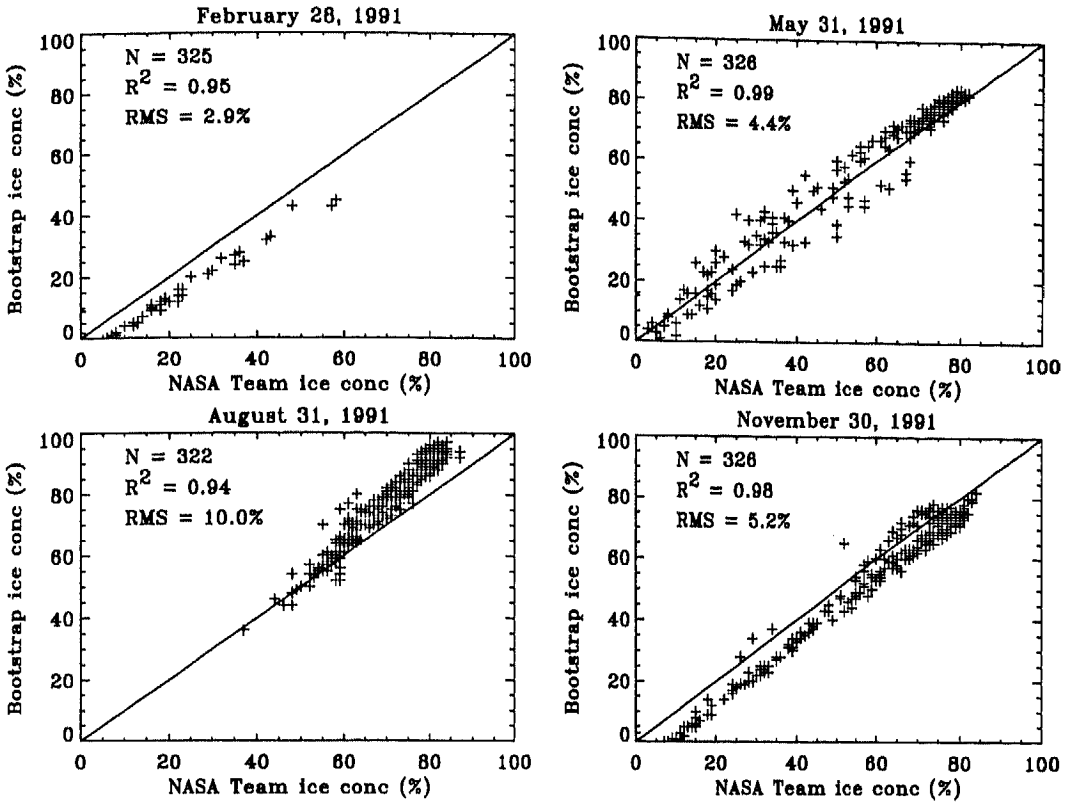

Fig. 3. Pixel by pixel comparison between NASA Team and Bootstrap derived ice concentrations (%) for the LTER region. For each comparison is given the number of pixels (N) used in the linear regression, the coefficient of determination (R^2), and the root mean square (RMS) difference. The ranges in RMS differences for each respective month were: 1.0-4.7% in February, 2.2-7.8% in May, 5.5-16.5% in August and 4.4-9.7% in November.

helps explain why regionally and temporally averaged comparisons between the two algorithms show fairly similiar estimates of ice extent and coverage. Overall, the greatest discrepancies between the two algorithms, when considering the LTER region only, appear to be during winter, when root mean square (rms) differences can be as large as 16.5%.

Differences in ice concentrations derived by the two algorithms can be attributed to the sensitivity of the 37 GHz channels to surface melt and/or flooding and to thin ice [*Comiso et al.*, 1984; *Comiso et al.*, 1992; *Emery et al.*, 1994]. Because the Bootstrap algorithm *operationally* depends on the 37 GHz channels to determine ice concentrations, it underestimates surface flooded or melting sea ice, but more accurately detects thin ice (< 3 cm) associated with fall freeze-up and polynyas [*Emery et al.*, 1994]. In a study comparing Arctic regional ice concentrations derived from the NASA Team algorithm and the Bootstrap algorithm, *Emery et al.* [1994] found that the NASA Team yielded: 5% higher ice concentrations overall, 8% higher ice concentrations during summer, 10% lower ice concentrations during fall, and 0.5% higher ice concentration during nonmelt periods. Thus, the higher overall ice coverage and higher ice extent in spring and summer predicted by the NASA Team algorithm could be due to flooded and/or melting snow/ice surfaces. It has been observed that Antarctic snow/ice surfaces during nonmelt periods are generally wet due to seawater flooding caused by a thick snow cover which depresses ice floe freeboards below the water line [*Comiso et al.*, 1992; *Jeffries et al.*, 1994b]. In addition, snow/ice surfaces in the MIZ are wet due to seawater flooding caused by wave action. In contrast, the higher ice concentrations predicted by the Bootstrap algorithm in fall and winter could be due to the greater sensitivity of the 37 GHz channels to thin ice which is often found at the ice edge during ice growth and in openings of the pack ice (e.g. leads and/or polynyas). Thus, neither algorithm, when used operationally, is optimal for *all* seasons. However, the performance of both algorithms can be improved by using seasonally and locally adjusted tie points and/or by adjusting either algorithm so that the 19 GHz data are used during melt periods and the 37 GHz data are used during ice growth or cold month periods [*Steffen and Schweiger*, 1991; *Emery et al.*, 1994; *Comiso and Ackley*, 1994].

Despite the differences in estimating sea ice concentrations, both algorithms capture similiar seasonal and interannual patterns in spatially and temporally averaged regional ice coverage and extent (Figure 2), which are the main focus of this study. This was found also to be the case for Arctic regional comparisons [*Emery et al.*, 1994]. Therefore, our analysis of

the spatial and temporal variability in ice coverage should not be biased due to our selection of the NASA Team algorithm over the Bootstrap algorithm. However, if one wanted to analyze the daily evolution or distribution of marginal ice zones, open and/or close pack regions, then a detailed consideration of differences between the two algorithms would be appropriate, and seasonal and regional adjustments to either algorithm should then be made.

3.2. Visible and Infrared Cloud Detection and Tie-Point Algorithm

Due to different radiative processes, open water and sea ice are easily distinguishable at visible and infrared frequencies under cloud-free conditions. AVHRR channels 1 and 2 detect solar radiance reflected by the earth's surface and clouds, and AVHRR channels 4 and 5 detect terrestrial and atmospheric (i.e., clouds) emitted radiance, while channel 3 detects both solar reflected and emitted radiance. Thus, open water appears dark in the visible due to low reflectance or albedo and warm in the thermal-infrared due to high thermal emission. In contrast, sea ice appears bright in the visible due to high reflectance and cold in the thermal-infrared due to low thermal emission. Shorefast, first-year and multiyear sea ice have the highest clear-sky albedos due primarily to snow cover [*Grenfell and Maykut*, 1977; *Allison et al.*, 1993]. The dryer and thicker the snow cover, the higher the albedo. Young sea ice (including light nilas) may have intermediate albedo values [*Allison et al.*, 1993], while new and thin sea ice less than 5 cm in thickness (i.e., grease ice, dark nilas and small pancakes) are nearly indistinguishable from open water at visible to near-infrared frequencies. However, new and thin sea ice can be distinguished from open water at thermal infrared frequencies [*Massom and Comiso*, 1994], although in the vicinity of marginal ice zones, open leads and polynyas, significant atmospheric water vapor and ice crystals may lead to the misinterpretation of new ice [*Steffen et al.*, 1993].

It is rare to have an AVHRR image of a region in the Southern Ocean which has both sea ice and open water and which is not contaminated by some clouds. In addition, clouds can not always be distinguished from underlying sea ice at visible and infrared frequencies, especially high level cirrus clouds and low level fog and stratus clouds [*Key and Barry*, 1989; *Steffen et al.*, 1993]. There have been many techniques devised for the detection and masking of clouds using visible and infrared imagery [*Steffen et al.*, 1993]. One such technique uses the difference between channel 3 and 4 radiances to produce a greater contrast between sea ice and clouds, in particular, thin cirrus and low clouds and fog [*Massom and Comiso*, 1994]. *Massom and Comiso* [1994] were successful in masking out clouds in Arctic AVHRR scenes by using the above technique and empirically adjusting cloud thresholds for each scene until the image was masked of clouds. However, *Massom and Comiso* [1994] note that low-level and sub-pixel clouds still remain ambiguous. This study will also utilize the difference between channel 3 and 4 radiances for cloud detection and masking.

Ice edge and concentration mapping and polynya and lead detection derived from AVHRR data are common practices in many ice forecasting operations. The ice charts produced from such operations are usually prepared by conventional manual interpretation methods. AVHRR data have also been used in validation studies, where either manual analysis, subjective classification techniques or objective automated routines are used to estimate ice concentrations. In most cases, both subjective and objective techniques are employed. For example, a sea ice concentration algorithm, originally developed by *Comiso and Zwally* [1982] for Landsat imagery, linearly interpolates sea ice concentrations using reference values for open water and 100% ice cover, values which are empirically derived from the scene in question. This algorithm assumes that only two surface types exist, open water and white ice (sea ice covered by snow), and values between these two reference points or tie-points are ice concentrations at sub-resolution. As with the NASA team algorithm, new and thin ice types are not uniquely determined and will either be misidentified as open water or low ice concentration. Another common technique used to calculate ice concentrations from visible and infrared imagery is the threshold method [*Steffen and Schweiger*, 1990; *Emery et al.*, 1991]. In this method different representative surface types are subjectively identified (e.g., open water/dark nilas, light nilas, gray ice, gray-white ice and white ice), and the image is then classified according to these representative values. The threshold method assumes that a pixel contains only one surface type, which may not be the case for the relatively large AVHRR pixel size (as compared to Landsat pixel size of 30 m). Thus, the tie-point algorithm will be used in this study. The tie-point algorithm is also analogous to the NASA Team algorithm from which the passive microwave ice concentrations are calculated, and to which the AVHRR ice concentrations will be compared.

Sea ice concentrations estimated from AVHRR imagery, whether it be through subjective or objective analyses, are limited by (1) cloud detection and masking of low-level and sub-pixel scale clouds, (2) discrimination between new/thin sea ice and open water in the vicinity of open leads and polynyas, and (3) interpretation of ice concentrations for pixels that include mixtures of ice types. The tie-point algorithm, as opposed to the threshold method, does account for sub-resolution mixtures of open water and white ice, but is limited by these two surface types. The tie-point algorithm, however, was preferred over the threshold method by *Steffen and Schweiger* [1990] and *Zibordi and Van Woert* [1993] for spring or summer conditions, because open water/dark nilas and white ice are the major surface classes, and because the results gave a more realistic distribution of sea ice concentrations. *Steffen and Schweiger* [1990] showed for an East Greenland scene, that SSM/I derived ice concentrations (using the NASA Team algorithm) overestimate ice concentrations relative to AVHRR derived ice concentrations (using the tie-point algorithm) by 9.6%. In a more recent study, *Emery et al.* [1994] used 16 nearly coincident SSM/I and AVHRR images from different Arctic regions and times of year to compute ice concentrations derived from SSM/I and AVHRR. They found that in comparison with AVHRR derived ice concentrations (using the tie-point algorithm), the NASA Team derived SSM/I ice concentrations underestimate by 6% during cold months and overestimate by 3% during summer. They also show that the tie-points used in determining AVHRR derived ice concentrations could be altered so that the differences between SSM/I and AVHRR

derived ice concentrations were negated. Thus, the subjective selection of tie-points used in the estimation of AVHRR ice concentrations contributes to the sources of error involved in comparing SSM/I and AVHRR derived ice concentrations.

4. METHODOLOGY

4.1. Passive Microwave Data Analysis

Southern Ocean ice concentrations were processed into monthly averages and then divided into regions. Percent surface concentrations were converted into regional sea ice coverages by multiplying the percent ice coverage for each pixel by the geographically corrected pixel area and summing pixel coverages for the region in question. Because the NSIDC grid is projected in a polar stereographic plane tangent at 70°S, pixel areas decrease north and increase south of 70°S, resulting in distortion. Thus, in the calculation of ice coverages, true pixel areas based on the geographic distortion of the projection were used. It should be noted that sea ice *coverage* is distinct from another sea ice parameter, sea ice *extent*. Sea ice extent is defined as the area bounded by an ice concentration contour corresponding to a given threshold (usually 15%). Thus, sea ice *extent* may include areas of open water as well as varying percentages of sea ice cover, whereas sea ice *coverage* is the total area of actual sea ice and is referred to as *area* in *Gloersen et al.* [1992]. Throughout this study, sea ice coverage is used exclusively and may be referred to simply as ice coverage. Image processing and time series analysis were performed using IDL (Interactive Data Language) and S-Plus, respectively.

The original analysis of spatial and temporal variability in Southern Ocean sea ice coverage [*Stammerjohn*, 1993] included 8 regions: Southern Ocean (as a whole), Weddell, Indian, West Pacific, Ross, Amundsen, Bellingshausen, and the LTER study area (Figure 1). The Weddell, Indian, West Pacific and Ross regions, and the combined Amundsen and Bellingshausen regions, were divided along the same lines as in *Zwally et al.* [1983] and *Gloersen et al.* [1992]. This study will focus primarily on the western Antarctic Peninsula, namely the LTER study area. The Southern Ocean, Amundsen and Bellingshausen regions (both combined and separate) and a subregion of the Weddell, the eastern Antarctic Peninsula (Figure 1), will be included for comparison and to illustrate the longitudinal spatial extent of temporal features along the western Antarctic continent. For higher frequency time series analysis, the Southern Ocean, Bellingshausen and LTER regional time series were reprocessed into 2-day averages. For *visual* comparison with AVHRR data, the corresponding SSM/I image for the day in question was re-projected into the stereographic projection of the AVHRR image.

4.2. Visible and Infrared Data Analysis

The HRPT data were converted from sensor counts to calibrated data using methods described by *Lauritson et al.* [1988]. Raw counts from channels 1 and 2 were converted to percent albedos using a linear relationship determined prior to launch. These calibration coefficients are downloaded with the HRPT data and are satellite dependent [*Kidwell*, 1991]. Raw counts from channels 3, 4 and 5 were converted to radiances using a linear relationship between the raw count value associated with cold space (approximately 3°K) and the raw count value associated with the temperature of an onboard target (approximately 300°K). A quadratic function was applied to channel 4 and 5 radiances to correct for a slight nonlinearity. Channel 3, 4 and 5 radiances were then converted to brightness temperatures using an approximation of the inverse of the Planck function. The images were then registered to a stereographic projection for visual analysis, and relatively cloud-free images of the western Antarctic Peninsula were selected. Image processing was performed using TeraScan software.

Out of 350 images screened from September to December 1991, only ten relatively cloud-free images for three separate time periods (September 12, September 30-October 1, and October 9-10) were found for the western Antarctic Peninsula. Six of the ten images had solar zenith angles (SZA's) between 60° and 82°, and the other four were at night. The September 30 image at 2136 GMT (SZA's between 78-82°) and the October 10 image at 1932 GMT (SZA's between 64-70°) were selected for the high and low resolution comparison, because both images contained pack ice, diffuse marginal ice zones and open water, and because ice concentrations could be derived from channel 2 reflectances. Only data collected within a sensor scan angle of ±50° were used from both images to minimize geometric distortion and angular dependence effects on albedo and emissivity. The two images were then imported into IDL along with the respective latitudes, longitudes and SZA's. The variation in reflectance across the image due to variation in SZA was corrected by dividing the albedos by the cosine of SZA. Using the cloud masking technique described in Section 3.2, pixels identified as cloudy were set to a nodata value. Ice concentrations were then estimated using the tie-point algorithm and projected into the NSIDC grid, binned to 25 km square cells and masked of land (using the NSIDC landmask) to allow for a pixel-by-pixel comparison with the respective SSM/I images.

5. RESULTS

5.1. Seasonal Variability

The time series of monthly ice coverage for the Southern Ocean, Amundsen and Bellingshausen (shown together and separately), LTER, and eastern Antarctic Peninsula regions are shown in Figure 4. The time series are dominated by strong, regular seasonal variations, upon which is superimposed the interannual variability in ice coverage. Variability in longitudinal sectors are often out of phase [*Stammerjohn*, 1993], so that the interannual variability for the Southern Ocean as a whole is relatively smooth. The five regions of the Southern Ocean shown in Figure 4 have several anomalous years in maximum and minimum ice coverage. High anomalous ice years, 1980, 1987 and 1990 and/or 1991, and low anomalous ice year, 1989, appear in the eastern Antarctic Peninsula, LTER and Bellingshausen regions, whereas high anomalous ice years, 1979, 1985 and 1989, and low anomalous ice years, 1980 and

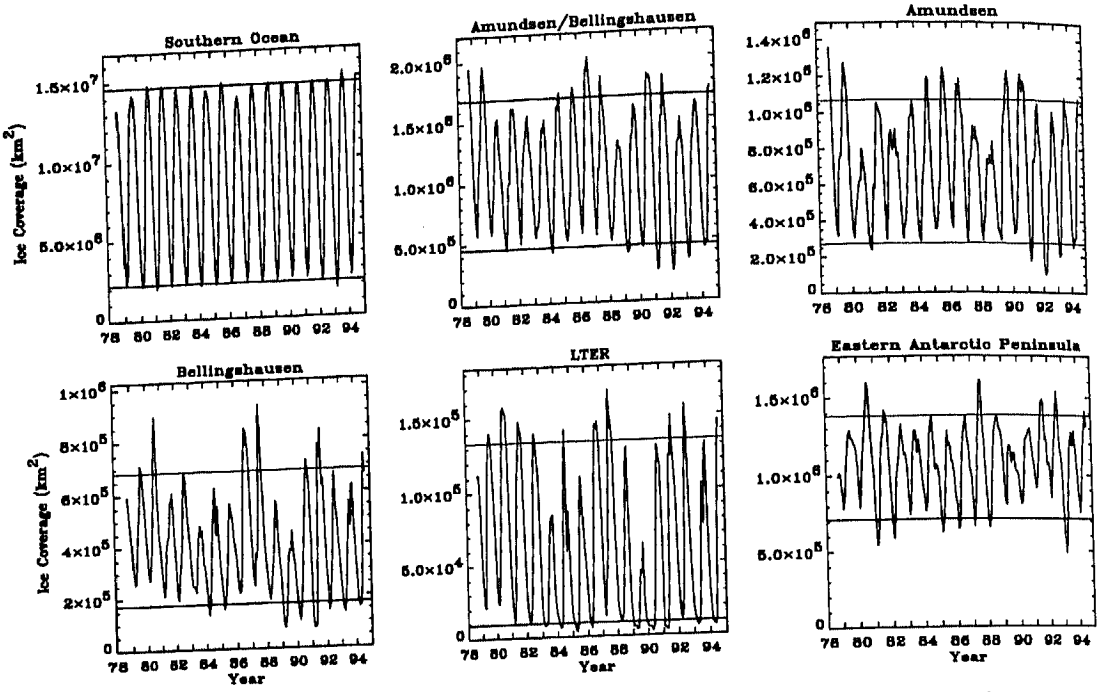

Fig. 4. Monthly ice coverage for selected regions of the Southern Ocean from October 1978 to August 1994. The horizontal lines are 15-year mean maximum and 16-year mean minimum ice coverages.

1988, appear in the Amundsen region. The LTER and Bellingshausen (which includes the LTER) regions show several more high and low anomalous ice years which are not apparent in either the eastern Antarctic Peninsula or Amundsen regions. Interannual variability in minimum ice coverage is also high and is very different for each region. The eastern Antarctic Peninsula region has the highest average minimum ice coverage due to larger amounts of multiyear ice coverage in that region, whereas minimum ice coverage in the LTER region is near zero in all but a few years.

As detailed in an earlier study [*Stammerjohn*, 1993], individual regions of the Southern Ocean show significant interannual variability in ice coverage, and no two regional time series had the same anomalous years of extreme maximum and minimum ice coverages. In contrast to the high regional interannual variability, the Southern Ocean as a whole shows little interannual variability. This confirms an early observation made by *Zwally et al.* [1983]. The consequence is that regional interannual variability in ice coverage appears to be a re-distribution of near constant ice coverage for the whole Southern Ocean.

5.2. Annual Cycles

The mean annual cycles for the six selected regions are shown in Figure 5. Two distinguishing characteristics illustrated by the shapes of the annual cycles are (1) the mean months of minimum and maximum ice coverage, and (2) the mean duration of ice advance and retreat. The mean month of minimum ice coverage is February for the Southern Ocean, Amundsen and eastern Antarctic Peninsula regions, March for the LTER and Bellingshausen regions, and February-March for the Amundsen/Bellingshausen region. September is the mean month of maximum ice coverage for the Southern Ocean, August for the Bellingshausen, LTER and eastern Antarctic Peninsula regions, September-October for the Amundsen region and August-September for the Amundsen/Bellingshausen region. For other Southern Ocean regions, such as the Weddell, Indian and West Pacific, February and September were the mean months of minimum and maximum ice coverage, respectively, whereas the Ross region had the same mean months of minimum and maximum ice coverage as the Amundsen region, February and September-October.

As a consequence of the different mean months of minimum and maximum ice coverage, the mean duration of ice advance and retreat also varies. The annual cycles for the eastern Antarctic Peninsula and Amundsen/Bellingshausen regions show symmetry with an approximate 5-6 month period of ice advance and retreat, whereas the other four annual cycles are not symmetric, including the annual cycle for the Southern Ocean. The Bellingshausen and LTER annual cycles are characterized by a shorter period of ice advance (approximately 5 months) followed by a longer period of ice retreat (approximately 7 months). In contrast, the Southern Ocean and Amundsen annual cycles show a longer period of ice advance (approximately 7 months) followed by a distinctly shorter period of ice retreat (approximately 4-5 months). The annual cycles of the Amundsen and Bellingshausen have opposite asymmetry, which explains the symmetry in the combined regional annual cycle. The other Southern Ocean regions were

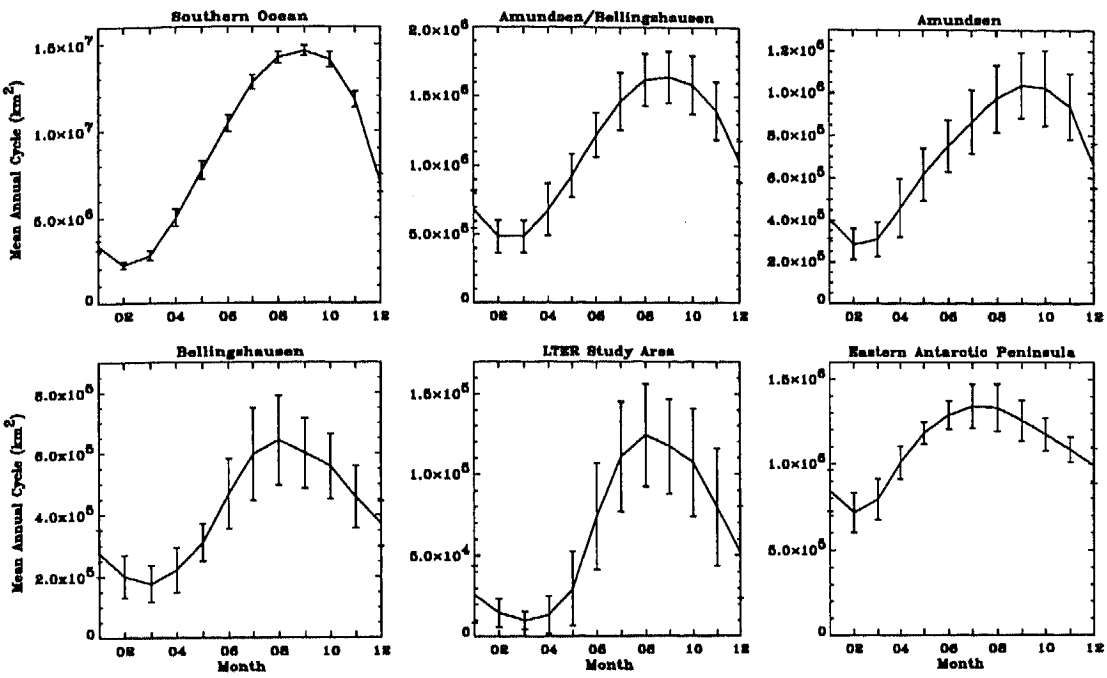

Fig. 5. Mean annual cycles for selected regions of the Southern Ocean based on the October 1978 to August 1994 monthly record. The annual curve represents a 16-year mean for all months except September which represents a 15-year mean. The vertical bars are one standard deviation above and below the mean.

also characterized by a longer period of ice advance followed by a shorter period of ice retreat, which agrees with an observation first made by *Zwally et al.* [1983]. It should be noted, however, that the Bellingshausen, LTER and Amundsen annual cycles show considerable year-to-year variability, therefore the shape of the mean annual cycles should be regarded cautiously. Mean monthly growth and decay rates were calculated for the eight regions in the original study, and except for the Bellingshausen and LTER regions, the highest rates were *decay* rates in December and January, showing dramatic *decreases* in ice coverage. In contrast, the highest rates for the Bellingshausen and LTER regions were *growth* rates in June and July, showing moderate to high *increases* in ice coverage.

To better resolve the year-to-year variability in the LTER mean annual cycle, a contour plot of each LTER annual cycle for the 15 complete years from 1979-1993 is illustrated in Plate 1. The year-to-year variability in the LTER annual cycle shows that near minimum ice coverage (dark blue area < 2.5 x 10^4 km^2) may persist for less than one month (1980) to more than seven months (1989). Near maximum ice coverage (red area > 1.25 x 10^5 km^2) may persist for less than one month (1988) to more than four months (1980), or in low ice years never reaching 1.25 x 10^5 km^2 (1983, 1985 and 1989). Year 1980 stands out as the highest ice year for the 15-year record, reaching a maximum ice coverage greater than 1.5 x 10^5 km^2 for at least three consecutive months. Years 1987 and 1992 are the only other years which reached a maximum ice coverage greater than 1.5 x 10^5 km^2. In these three high LTER ice years, the sea ice extended out into the Drake Passage to about 58°S. The rates of ice advance and retreat are also different for each year. All years except 1993 and the two lowest ice years, 1983 and 1989, show the same asymmetry observed in the mean annual cycle, a shorter period of ice advance followed by a longer period of ice retreat. In years 1983, 1989 and 1993, the period of advance is longer than the period of retreat. Years 1984 and 1993 are particularly unusual in that they show two periods of ice advance. Years 1984, 1985, 1988, 1990, 1991 and 1993 show long periods of minimum ice coverage from January to approximately May followed by dramatic increases in ice coverage. Years 1983 and 1989, the two lowest ice years, also show long periods of minimum ice coverage, but the increase in ice coverage in fall is not as dramatic. The contour plot in Plate 1 shows in particular the oscillation between consecutive high ice years followed by consecutive low ice years. For example, two to four high ice years (1979-82, 1986-87, 1991-92) are followed by one to three low ice years (1983-85, 1988-90, 1993), a pattern suggestive of a 5-7 year periodicity in high ice.

The distribution of ice throughout the LTER study area from year-to-year is consistent in that ice advances from the southwest toward the northeast and from the peninsula toward the northwest. In July-October 1980, August 1981, July 1987 and August 1991, the entire LTER region was covered with greater than 50% ice coverage. Year 1980 was again particularly remarkable in that the high ice coverage lasted four months as opposed to one month in the other three years. In near normal ice years, the ice coverage advances to just south of Anvers Island and extends northwestward across the study area. From January to April there is little ice coverage in about 90% of the LTER study area, thus mean summers are long for

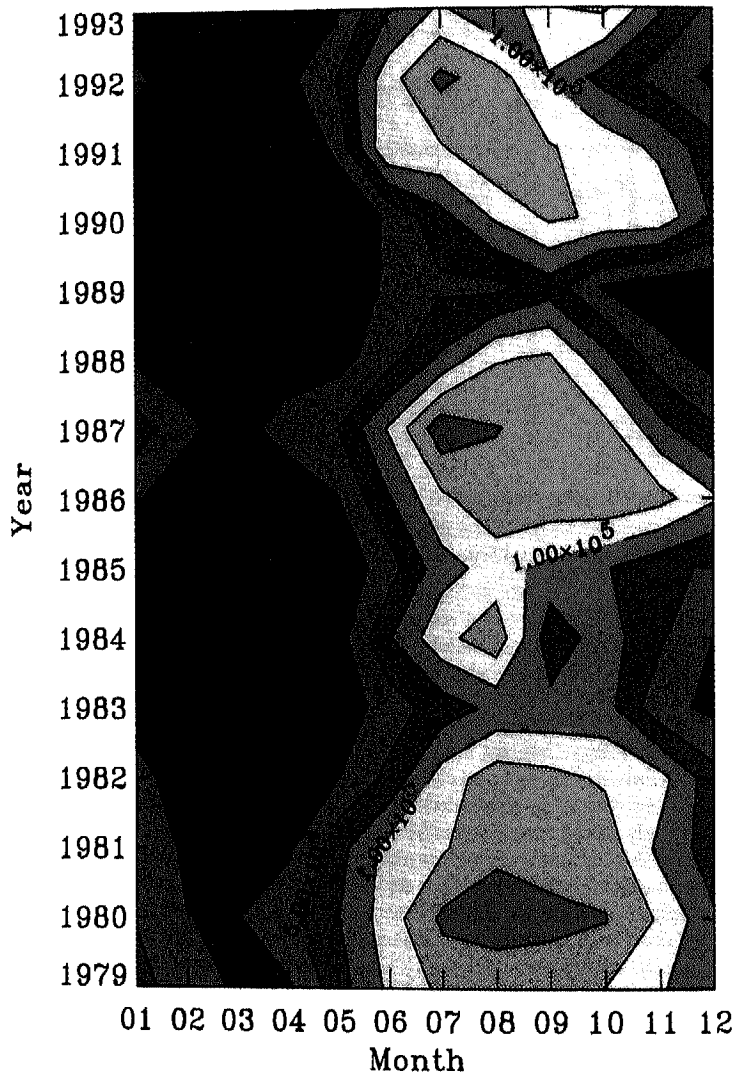

Plate 1. Contour plot of LTER annual cycles for years 1979-1993. Contours are labeled with ice coverages in km^2.

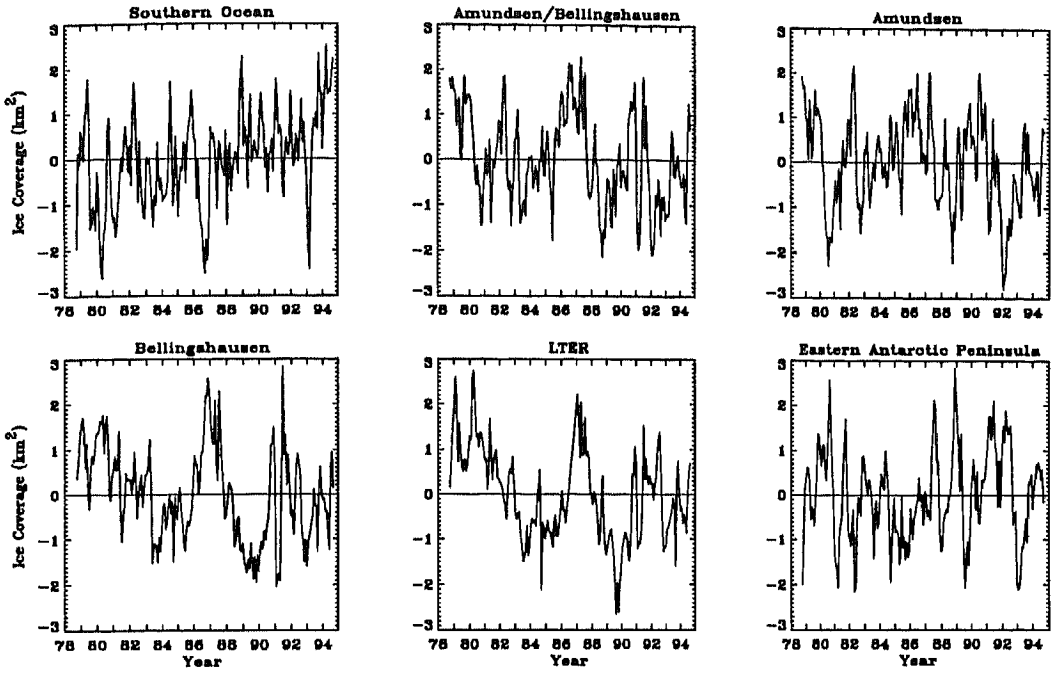

Fig. 6. Standard deviates of monthly anomalies for selected regions of the Southern Ocean from October 1978 to August 1994.

the LTER region. The vicinity of Anvers Island and northeast along the coast is often ice free during maximum ice coverage, and in high ice years (e.g., 1981, 1986, 1987, 1991) this area marks the location of a near coastal polynya which varies in size on a daily basis. In extreme low ice years (1983 and 1989), maximum ice coverage extends diagonally from about 200 km south of Anvers Island across to about 200 km north of the lower left corner of the study area. Thus, the southern region of the LTER study area experiences the most consistent ice coverage from year-to-year, whereas the northern third of the LTER study area, in particular, the vicinity and northeast of Anvers Island, experiences the most dramatic fluctuations in year-to-year ice coverage. This high variability in ice coverage in the vicinity of Anvers Island provides the Palmer LTER with an ideal study site in which to conduct "natural experiments" associated with the high interannual sea ice variability and the hypothesized consequences to the marine ecology of the area.

5.3. *Non-Seasonal Variability*

with ice

The monthly anomalies have the annual cycle removed and thus represent the non-seasonal variability in ice coverage. Figure 6 shows the time series of the normalized monthly anomalies for the six selected regions. The monthly anomalies were normalized by subtracting the mean and dividing by the standard deviation. The Southern Ocean, Amundsen and eastern Antarctic Peninsula non-seasonal time series oscillate consistently from above average to below average monthly values on time scales of a few months to a year, or in a few cases, up to nearly two years. In contrast, the Bellingshausen and LTER non-seasonal time series oscillate fairly consistently from above average to below average monthly values on time scales of a few years, a pattern observed in the LTER annual contour plot (Plate 1). Autocorrelations calculated from the monthly anomalies for all the Southern Ocean regions support the above observations in that autocorrelations for all regions except the Indian, Ross, Bellingshausen and LTER regions become insignificant within 4-5 monthly lags. For the Indian, Ross, Bellingshausen and LTER regions, monthly lags are significantly autocorrelated up to 8, 16, 13 and 17 months, respectively. However, the Indian and Ross monthly anomalies do not show a clear pattern of above mean years followed by below mean years, as does the Bellingshausen and LTER monthly anomalies. In the original analysis [*Stammerjohn*, 1993], the Southern Ocean was divided into 15° longitudinal pie sections to determine whether any other LTER-sized region shows such patterns of interannual variability in anomalous ice coverage, but only the pie section including the LTER study area showed the above mentioned multiyear pattern.

Cross spectral analysis of a subregion containing the LTER study area (60-77°W) versus 10° longitudinal pie sections to the east and west of the LTER subregion was performed to determine the longitudinal spatial extent of coherence. Figure 7 shows the squared coherence between the LTER and six subregions. The top two plots are squared coherences against two subregions to the east of the LTER subregion (i.e., east of the Antarctic Peninsula), which show little significant coherence. This is consistent with expectations, since both sea ice and meteorological conditions are known to be significantly different on the two sides of the peninsula [*Schwerdtfeger*, 1975; *Schwerdtfeger*, 1984]. There is however significant coherence against the first two subregions to the west of the LTER subre-

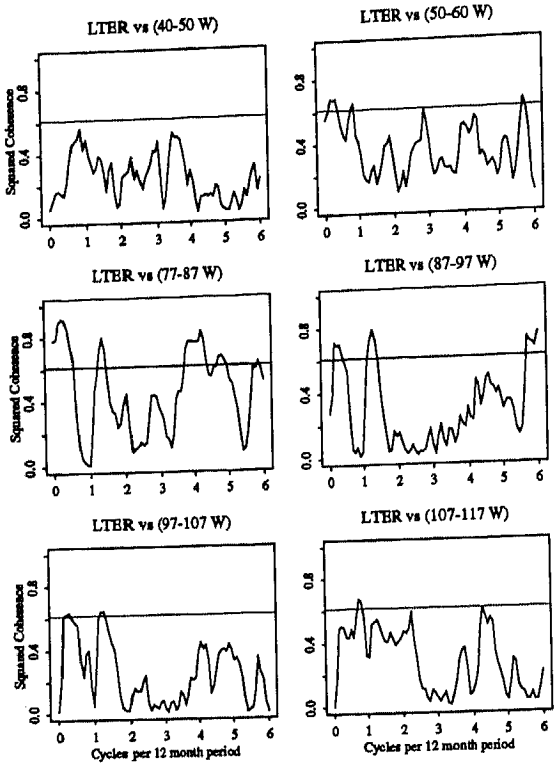

Fig. 7. Squared coherence of monthly deseasonalized anomalies between the LTER subregion (60-77°W) and six subregions near the LTER. The dotted line indicates the 0.01 significant level for the null hypothesis that the true coherence is zero.

gion (the middle two plots) which together include a 20° longitudinal distance from the west boundary of the LTER subregion. The phase spectrum indicates that the two regions west of the LTER subregion are slightly out of phase and leading, indicating that the propagation of coherence is from west to east. Beyond a longitudinal distance of about 97°W, there is no significant coherence (the bottom two plots). In general, the cross spectral analysis suggests that variability in ice coverage for the LTER study area is not characterized by variability east of the Antarctic Peninsula but may be characterized by variability west of the Antarctic Peninsula to about 97°W. In addition, cross spectral analysis performed on the other Southern Ocean regions showed low frequency coherence between the Amundsen and Bellingshausen monthly anomalies. The phase angle indicates a 9-11 month difference, with the Amundsen leading. Therefore, anomalous ice coverage in the Amundsen is similar to anomalous ice coverage in the Bellingshausen a year later.

An analysis of higher frequency variance was conducted for the Southern Ocean, Bellingshausen and LTER regions [*Stammerjohn*, 1993]. The time series were processed into 2-day averages and divided into four seasons to better resolve possible high frequency periodicities which may occur only at certain times of the year. Figure 8 shows the LTER autospectra, and there is one distinct peak in summer at approximately 16 cycles per 90-day season, which translates into a 5-6 day periodicity in the variability of summer LTER ice coverage. This peak was also prominent in the Southern Ocean summer autospectrum and detectable in the LTER fall autospectrum and in the Bellingshausen summer and winter autospectra.

5.4. High and Low Resolution Comparison

Visual comparisons of western Antarctic Peninsula spring ice cover are made between AVHRR channel 2 albedos and SSM/I derived ice concentrations in Plates 2 and 3. Features in the MIZ or leads and polynyas which have dimensions greater than 1 to 2 km will be resolved in AVHRR imagery but are not resolved in passive microwave imagery, unless the dimensions are at least 30 to 70 km, depending on the passive microwave frequency. For example, the September 30 AVHRR image (Plate 2) shows a distinct swirl (about 130 km wide and 210 km long) in the MIZ northwest of Adelaide Island. The outline of this feature is detectable in the SSM/I image, but the swirling pattern is lost with the lower resolution. Other features notable in the September 30 AVHRR image are the numerous fine lines or leads in the ice pack. These leads are just barely detectable and are on the order of 2 to 3 km wide, and many of them appear to be covered by new or thin sea ice, while only a few show open water albedos. There are larger open leads (approximately 5-8 km wide) just northwest of Alexander Island and a polynya (approximately 12 by 20 km) southwest of Adelaide Island, which appear to be openings between the fast ice extending toward the coastline and the open pack ice extending toward the MIZ. The area just east of Adelaide Island and adjacent to the peninsula shows a small polynya (5 by 5 km) next to a 20 km region (stretching to the southwest) of low albedos indicating new or young sea ice.

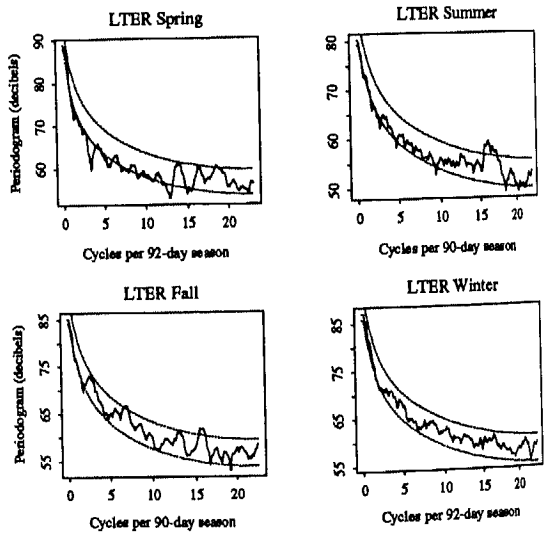

Fig. 8. LTER autospectra generated from 2-day time series of deseasonalized anomalies. The dashed lines represent 95% confidence intervals for autospectra generated from first order autoregressive models.

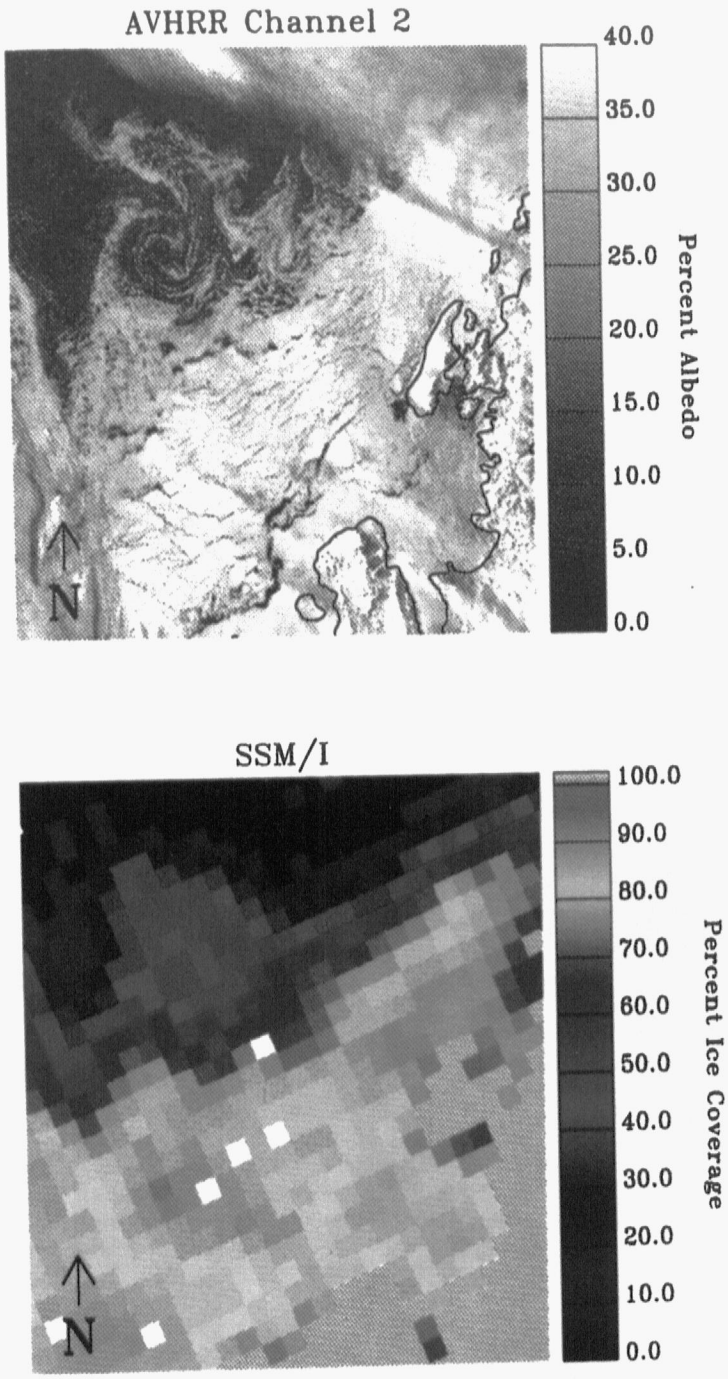

Plate 2. High resolution AVHRR channel 2 image of ice coverage north of Adelaide and Alexander Islands contrasted with the low resolution SSM/I image of the same area on September 30, 1991. The islands and western Antarctic Peninsula are outlined in black in the AVHRR image and masked in gray in the SSM/I image. White pixels represent no data in the SSM/I image, and clouds have not yet been masked in the AVHRR image.

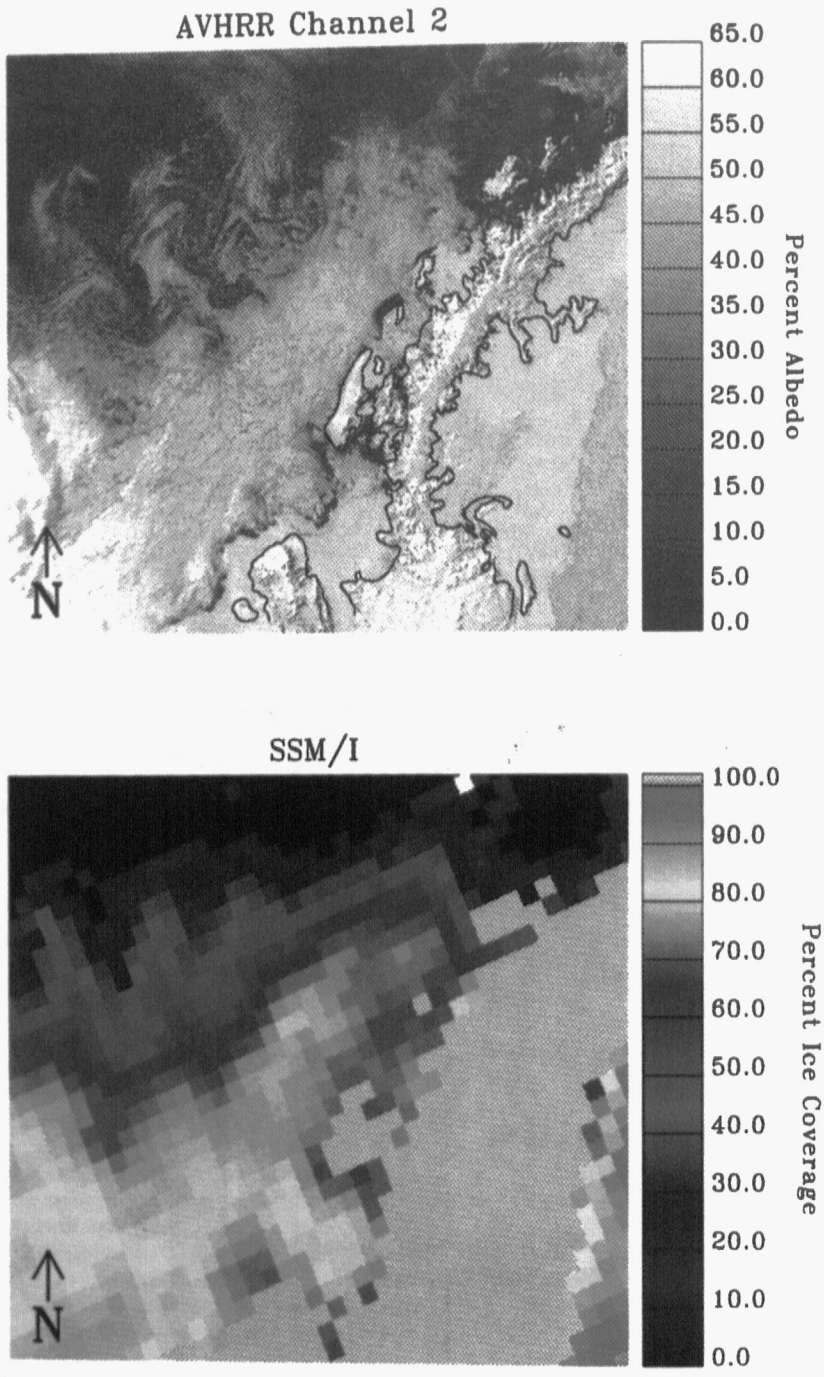

Plate 3. Same as in Plate 2 but for October 10, 1991.

These larger leads and polynyas which are apparent in the AVHRR image are not large enough to be well represented in the SSM/I image. At best, the SSM/I image shows ice concentrations ranging from 55-70% in these polynya areas, which is a decrease from 70-90% outside these areas.

The October 10 AVHRR image (Plate 3) shows an ice margin that is again highly diffuse and extending approximately 200 km from the main pack ice. The features in the MIZ as depicted in the AVHRR image are again reflected in the lower resolution SSM/I image, although at what appear to be higher sea ice concentrations. As in the September 30 AVHRR image, the ice pack appears to be a mixture of consolidated sea ice and frozen over leads. There are again open leads northwest of Alexander Island, and the polynyas to the southwest and east of Adelaide Island have increased in size. A relatively large polynya (approximately 15 by 40 km) opened west of Lavoisier Island (the small island north of Adelaide Island and south of Renaud Island) and a smaller one north of Renaud Island. Again, none of these open leads or polynyas are large enough to be resolved in the SSM/I image, but are suggested by the lower ice concentrations estimated by the NASA Team algorithm.

The September 30 and October 10 AVHRR images were compared to the same-day SSM/I images to determine which SSM/I ice concentration contour best corresponded to the AVHRR diffuse ice edges. In both instances, the 20% SSM/I ice concentration contour best identifies the northernmost bands of ice in the AVHRR images, but fails to follow the convoluted structure in the diffuse ice edge, especially in the October 10 AVHRR image. The 30% SSM/I ice concentration contour better follows the convolutions in the ice edge, but can be up to 25-50 km south of the northernmost bands of ice. The 75% SSM/I ice concentration contour appears to best follow the outline of the main pack ice, which, as shown in Plates 2 and 3, appears to be a mixture of consolidated sea ice and frozen over leads.

Ice concentrations were calculated from September 30 and October 10 AVHRR channel 2 reflectances and projected into the NSIDC polar stereographic grid and binned to 25 km square pixels, to facilitate comparison with the same-day SSM/I images. As shown in Plate 4, the AVHRR ice concentration image shows a more spatially varying ice cover than the SSM/I ice concentration image. AVHRR predicts much lower ice concentrations in the MIZ, however there is modest agreement between ice concentrations in the main pack ice with some notable exceptions. The relatively wide open lead northwest of Alexander Island and polynya just southeast of Adelaide Island are still apparent in the AVHRR image (showing 0-20% ice concentrations), even at the 25 km bin size. There is also an area between Adelaide and Alexander Islands that extends north of the southern tip of Adelaide Island which shows ice concentrations in the 40-50% range in the AVHRR image contrasted with 80% ice concentrations in the SSM/I image. This discrepancy may be due to low level fog or cloud which was not detected in the AVHRR image. The presence of low fog or cloud would lower the albedo and falsely indicate lower ice concentrations. This area of lower albedos can be seen in Plate 2 as well, appearing somewhat like a shadow.

Plate 5 shows the October 10 ice concentration images. The areal extent of comparison is larger than in the September 30 comparison, but there are more clouds masked within the area of comparison as indicated by white. Again, the AVHRR ice concentration image shows a more spatially varying ice cover, as well as lower ice concentrations in the MIZ. However, there is a distinct trend towards higher AVHRR ice concentrations in the vicinity of the peninsula which is not reflected in the SSM/I image. Overall, it appears that in both the September 30 and October 10 comparisons, the 50% ice concentration contour shows the best agreement between the AVHRR and SSM/I ice concentration images.

Plate 6 shows the difference images obtained from subtracting SSM/I from AVHRR channel 2 derived ice concentrations for September 30 and October 10. The majority of differences for September 30 is negative and in the range of -25% to 0%, with a mean difference of -18.3% ±17.9%. The few areas which show positive differences are in the range of 0% to 10% and are located in the middle of the ice pack and northeast of Adelaide Island. The majority of differences for October 10 is also negative but with a lower mean difference of -9.8% ±18.1%. In the October 10 difference image, the areas of lower ice concentrations, as in the MIZ and an area adjacent and south of the MIZ, are marked by negative differences in the range of -25% to 0%, whereas the areas of higher ice concentrations, as in the area adjacent to the peninsula and in the vicinity of Adelaide and Alexander Islands (i.e., the southernmost region in the image), are marked by positive differences in the range of 0% to 10%. This pattern is shown more clearly in the scatter plots for the September 30 and October 10 comparisons in Figure 9.

6. DISCUSSION AND SUMMARY

6.1. Temporal and Spatial Patterns in the LTER Study Area

Interannual variability in monthly ice coverage is high for the LTER region, as well as for other regions of the Southern Ocean. For example, monthly maximum and minimum ice coverage in the LTER region can deviate up to 66% and 130% from mean maximum and minimum ice coverage, respectively. In contrast, the Southern Ocean as a whole exhibits little interannual variability, and monthly maximum and minimum ice coverage deviate at most by 4% and 12%. Thus, there is significant regional interannual variability, which appears to be a re-distribution of near constant ice coverage for the whole Southern Ocean. No two of the six main regions of the Southern Ocean have the same anomalous years of extreme maximum or minimum ice coverage, leading to asymmetries in Southern Ocean ice coverage.

The LTER study area is a sub-region of the Bellingshausen region, and it has been shown that annual and interannual variability in these two regions are very similar. Results from cross spectral analyses show that the region west of the Antarctic Peninsula to about 97°W is fairly homogeneous with respect to interannual variability in ice coverage. On the other hand, there is no coherence between the west and east sides of the Antarctic Peninsula. In fact, the ice regimes on the two sides of the peninsula are completely different. The east side of the peninsula is characterized by permanent ice fields, the Larson and Ronne-Filchner ice shelves and high concentra-

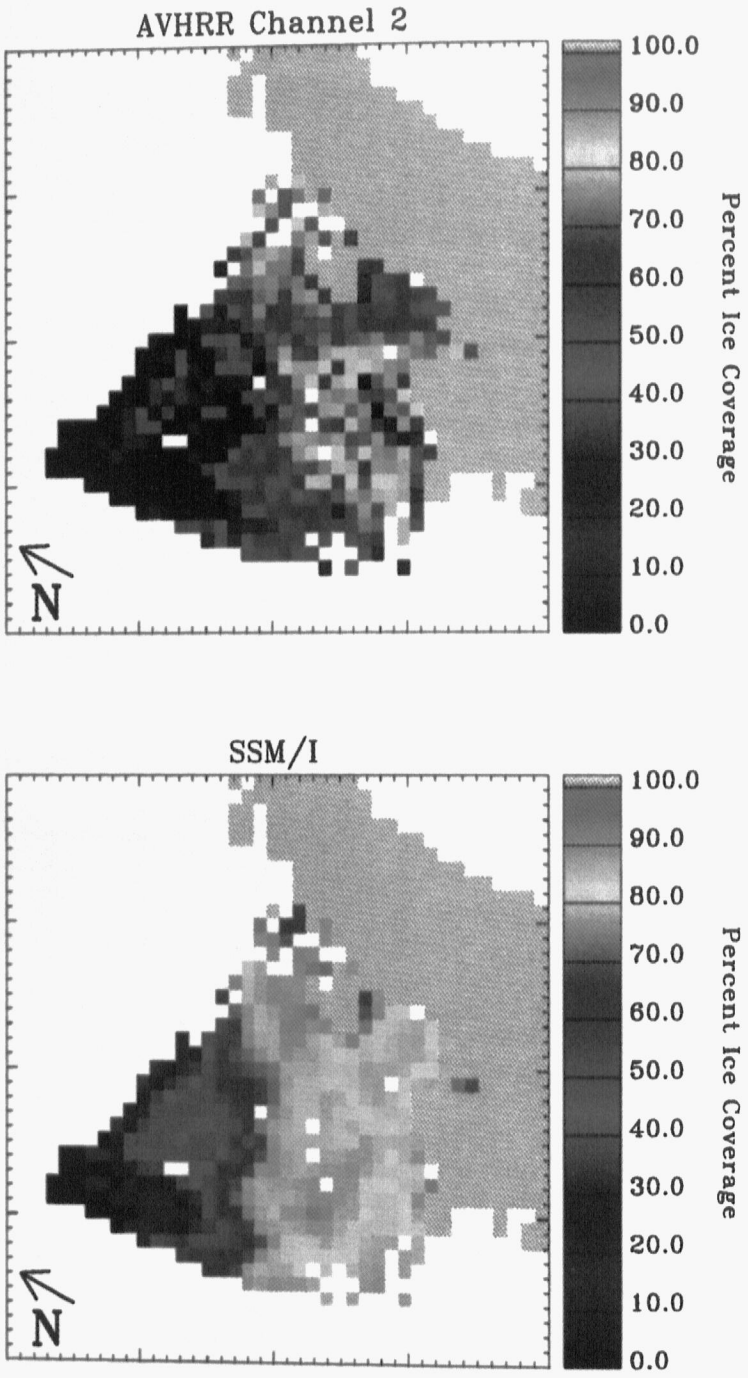

Plate 4. AVHRR channel 2 and SSM/I derived ice concentrations for September 30, 1991. Ice concentrations are projected in the NSIDC polar stereographic grid and binned to 25 km^2 pixels. Gray represents the NSIDC landmask and white indicates no data. Cloudy pixels are not included in the ice concentration calculations and are represented also as white pixels.

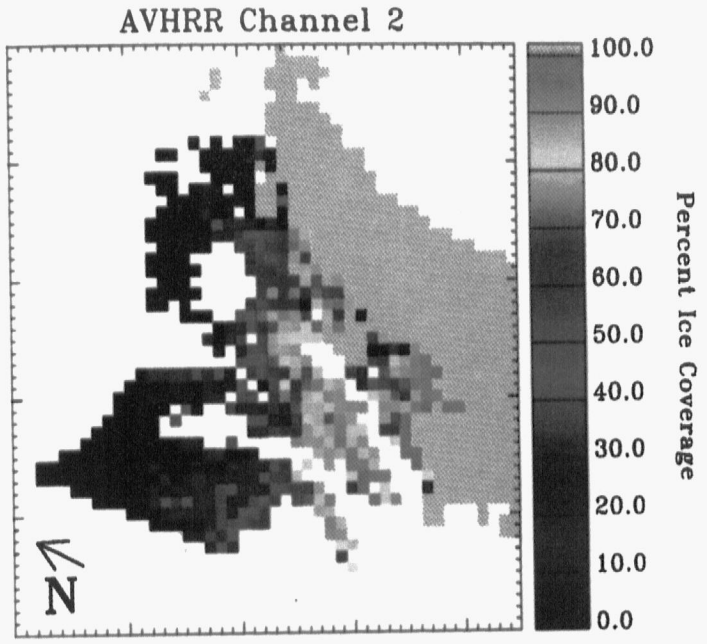

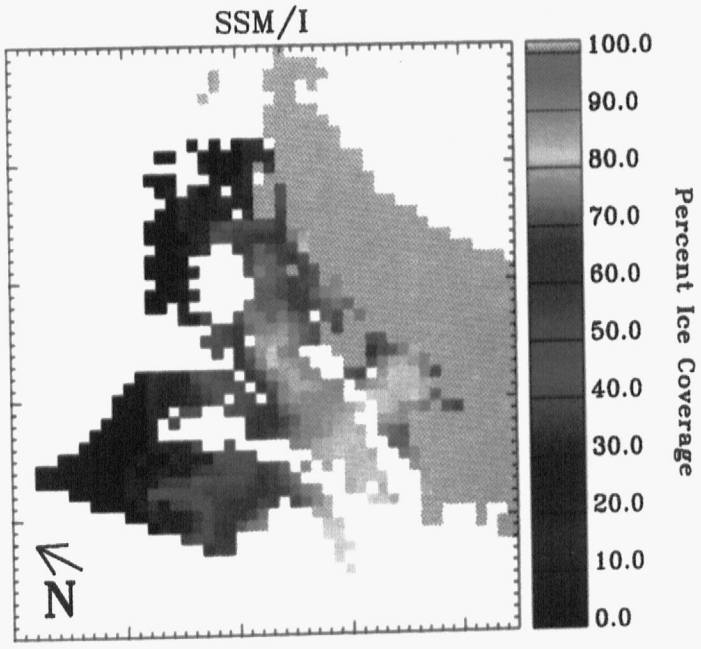

Plate 5. Same as in Plate 4 but for October 10, 1991.

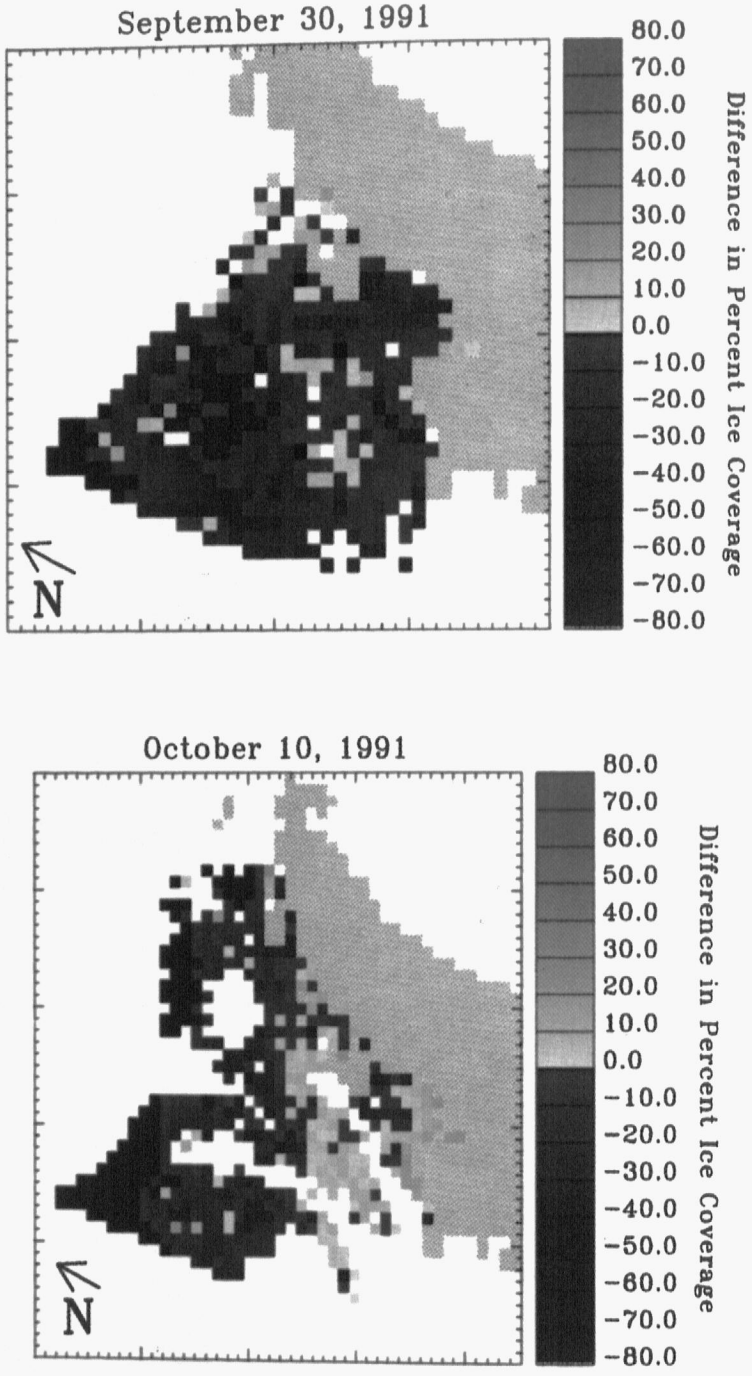

Plate 6. Difference images obtained from subtracting SSM/I from AVHRR channel 2 derived ice concentrations for September 30 and October 10, 1991. Gray represents the NSIDC landmask, white indicates no data and black indicates 0% difference.

tions of multiyear sea ice, and interannual variability is restricted to a seasonal ice zone northeast of these permanent ice fields. In contrast, the entire west side of the peninsula is characterized by a seasonal ice zone which has considerable interannual variability. Different atmospheric forcings can help explain the differences in ice regimes to either side of the peninsula [*Schwerdtfeger,* 1975; *Schwerdtfeger,* 1984]. Either a central low over the Weddell Sea or the barrier winds associated with the eastern Antarctic Peninsula mountain range help to maintain the permanent ice fields to the east of the peninsula by advecting cold air from the south. [*Schwerdtfeger,* 1975; *Ackley,* 1979; *Zwally et al.*, 1983; *Schwerdtfeger,* 1984]. No such persistent low or barrier winds are associated with the western Antarctic Peninsula region, rather longitudinal variability in location and frequency of lows to the west of the peninsula is considerably high [*Carleton,* 1981]. The location of these lows may influence whether the Bellingshausen experiences a high or low ice year. A low positioned over the Bellingshausen region will promote low latitude warm air advection into the region west of the peninsula, inhibiting ice growth, but a low positioned over the Amundsen region could advect ice zonally into the Bellingshausen region. Both scenarios have been observed by *Carleton* [1981] and *Parkinson and Cavalieri* [1982].

Thus, high interannual variability in LTER ice coverage can in part be explained by high interannual variability in the location and frequency of low pressure systems. For example, *Carleton* [1981], in a study on ice-ocean-atmosphere interactions at high southern latitudes, noted the following.

1. Winter cyclogenesis in the Southern Ocean is located close to the Antarctic Polar Front (APF; Carleton refers to this as the Oceanic Polar Front), a zone of steep latitudinal temperature gradients which borders the equatorward side of the Antarctic Circumpolar Current and is located near 50°S in all regions except the South Pacific (i.e., the Bellingshausen, Amundsen and Ross regions), where it is located near 60°S.

2. As cyclones mature, they migrate southeastward, and the maximum poleward extent of cyclone activity occurs in September (60-75°S).

3. In the Bellingshausen and Amundsen regions the influence of the APF on cyclogenesis is augmented by the close proximity of maximum winter sea ice coverage which reaches a mean latitude of 65°S. Nowhere else in the Southern Ocean is the APF located within 5° of maximum ice extent, except for a narrow region east of Victoria Land (a point of land west of the Ross Sea).

4. In these regions where the APF is in close proximity of maximum ice extent, a seasonal baroclinic zone develops near the ice margin which favors *in situ* cyclogenesis. These cyclones are often joined by cyclones migrating from lower latitudes in the South Pacific, resulting in a region of high interannual variability in both location and frequency of cyclones. The north Ross Sea and Bellingshausen regions showed the greatest interannual variability in cyclone frequencies for 1973-1977 winters.

The high variability in location and frequency of cyclogenesis in the Amundsen/Bellingshausen region may explain also why the interannual variability in Bellingshausen ice coverage is distinctly different from interannual variability in Amundsen ice coverage. Cross-correlation and cross spectral analysis between the Amundsen and Bellingshausen monthly anomalies

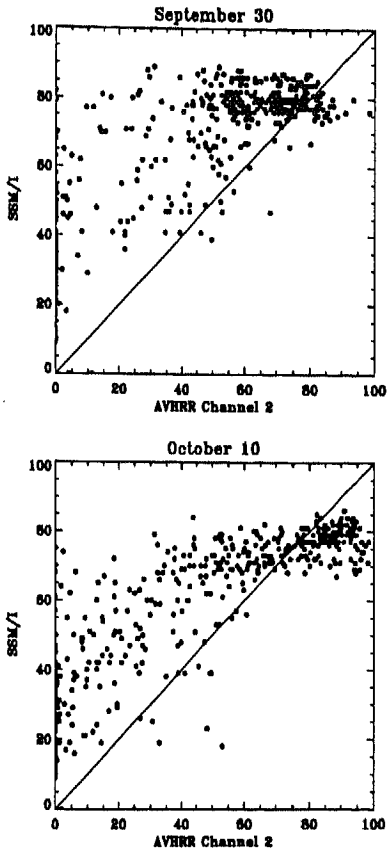

Fig. 9. Scatter plots of SSM/I versus AVHRR channel 2 derived ice concentrations for September 30, 1991 (n=458, R^2=0.64) and October 10, 1991 (n=551, R^2=0.74). The diagonal line represents a 1:1 comparison.

indicated that ice coverage in the Bellingshausen lagged ice coverage in the Amundsen by 9-12 months, or approximately one year, between winter ice coverages. This approximate yearly lag could be due to prevailing low pressure systems in winter which in one year may be more frequent in the Amundsen region and in the other year more frequent in the Bellingshausen region. Other studies have observed similar patterns between the Amundsen and Bellingshausen ice extents and low pressure systems and the eastward propagation of anomalies [*Cavalieri and Parkinson,* 1981; *Parkinson and Cavalieri,* 1982; *Chapman and Walsh,* 1993; *Jacobs and Comiso,* 1993].

Several distinguishing features of the oceanic environment west of the Antarctic Peninsula are described by *Hofmann et al.* [this volume], which may contribute to the sea ice variability in this region as well. For example, the most prominent water mass west of the Antarctic Peninsula is Circumpolar Deep Water (CDW), which is characterized by temperatures greater than 0.5°C and by salinities of 34.75. CDW is advected onto the shelf in response to the equatorward Ekman transport of surface waters. It is thought that the deeper shelf facilitates advection of CDW onto the shelf, where, as shelf

bottom water, it remains intact since wind mixing over the deep shelf is restricted to a shallower portion of the water column (about 150 m). In winter the upper part of CDW is within the mixed layer depth, allowing intrusion of warm, saline waters into the upper water column, where it may moderate sea ice production, as well as climate [*Hofmann et al.*, this volume]. Upwelling of warmer water in winter would lead to a thinner ice cover, as well as increase the frequency of coastal leads and polynyas. If the ice cover to the west of the Antarctic Peninsula is in fact thinner, then it would be more susceptible to wind-driven circulation.

Differences between regional annual cycles may indicate differences in regional oceanic and atmospheric forces as well. The Weddell, Indian, West Pacific, Ross and Amundsen mean annual cycles all show a 7 month period of ice advance followed by a 4-5 month period of ice retreat, with December having the highest overall monthly *decay* rate. In contrast, the Bellingshausen and LTER mean annual cycles show a 5-month period of ice advance followed by a 7-month period of ice retreat, with June having the highest overall monthly *growth* rate. *Hibler and Ackley* [1983] concluded from numerical simulations of the Weddell pack ice that ice advance is mostly driven by thermodynamics and that ice retreat is mostly driven by advective processes (resulting in open leads within the pack ice, which allows radiative heating of surface waters, which in turn melts the surrounding pack ice). It may be that these processes are reversed in the Bellingshausen region. For example, if more ice is advected into the Bellingshausen region than is grown *in situ*, and if more ice is melted *in situ* than is advected out of the region, then this could explain the short period of ice advance followed by the long period of ice retreat. This is supported in part by analyses of sea ice properties and growth processes in the Bellingshausen and Amundsen Seas which indicate that turbulent conditions prevail during sea ice development and that the relatively calm conditions promoting congelation ice growth by thermodynamic processes are neither common nor prolonged [*Jeffries et al.*, 1994b; *Jeffries et al.*, 1994a].

Another explanation for the opposite asymmetry observed in the Bellingshausen annual cycle is offered by *Harangozo* [1994], who analyzed possible links between ice extent and meridional circulation in the vicinity of the western Antarctic Peninsula region. The mean meridional circulation (1952-82) in the northern region of the western Antarctic Peninsula follows a semi-annual cycle where anomalous *equatorward* flow occurs from May to July (promoting a short period of ice advance) and anomalous *poleward* flow occurs from August to November (promoting ice compaction and decreasing rapid melting through equatorward advection). Thus, seasonal and interannual variability in sea ice in the western Antarctic Peninsula region may be explained in large part by the variability, persistence and strength of the meridional component of geostrophic flow.

Harangozo [1994] also points out that changes in the strength and persistence of the meridional component of the geostrophic flow may ultimately be manifestations of regional and even large-scale circulation changes in the southern hemisphere and consequently would determine winter sea ice anomaly development in the western Antarctic Peninsula region. This supports a finding made by *Smith et al.* [this volume] which found a strong anticorrelation between LTER sea ice extent and the Southern Oscillation Index (SOI). That study also found both low and high frequency coherence between Faraday air temperatures and SOI (in-phase) and between Faraday air temperatures and LTER sea ice extent (out-of-phase). Their conclusions suggests that not only do extreme events of ENSO affect the climate of the western Antarctic Peninsula, but monthly ENSO fluctuations appear to be affecting monthly anomalies in air temperature and sea ice extent as well. In addition, these strong ENSO signals detected in the western Antarctic Peninsula region are apparently an expression of circumpolar ENSO signals in sea surface temperature, meridional surface winds and sea ice extent which propagate eastward by the Antarctic Circumpolar Current, taking 8-10 years to circle the Antarctic continent [*W. B. White and R. G. Peterson*, personal communication, 1995].

The 15.9-year record is not nearly long enough to resolve possible long term trends in ice coverage, and spectral analysis shows that the variability in all regional monthly anomalies exhibits pure persistence (i.e., most of the variance is due to interannual variability). However, the time series of the Bellingshausen and LTER monthly anomalies (Figure 6) reveals a distinguishing multiyear pattern, resulting in a 5-8 year difference between extreme high ice years (1980, 1987 and 1992). The ice record is not long enough to test the significance of a 5-8 year periodicity, but spectral analysis was performed on the 1945-90 air temperature record from Faraday Station, against which LTER ice extent highly correlates [*Smith et al.*, this volume]. A broad peak centered at a 5 year periodicity was prominent in the air temperature autospectrum but was just below the 95% confidence level. This suggests that either the record is still too short or that the frequency of high ice/low temperature years may be aperiodic, which is consistent with the finding of ENSO linkages.

The 15.9-year record is however long enough to discern any high frequency periodicities. Spectral analysis of 2-day time series of each season indicated that there may exist an approximate 5-6 day periodicity in anomalous ice coverage. The 5-6 day signal was strongest for the Southern Ocean and LTER summer autospectra, but was also detectable in the Bellingshausen winter and LTER fall autospectra as well. Spectral analysis was performed also on daily anomalous air temperatures from Faraday Station [*Smith et al.*, this volume] which showed several periodicities in the 4 to 8 day range and which were strongest in summer and fall autospectra. Whether these periodicities in both ice coverage and air temperature are related to quasi-periodic passages of low pressure systems across the western Antarctic Peninsula region remains to be determined from further analysis using higher resolution ice data (preferably SAR) and regional climatologies.

6.2. High Versus Low Resolution Perspective

Comparisons between high resolution AVHRR and low resolution SSM/I imagery show that for a highly diffuse ice edge, the 20% SSM/I ice concentration contour best identified the northernmost bands of sea ice in the AVHRR imagery but failed to follow the convoluted structure in the diffuse ice edge. The 30% SSM/I ice concentration contour better followed the convolutions but can be up to 50 km south of the northernmost bands of sea ice, and the 75% SSM/I ice concentration contour

coincided with the outline of the main pack ice. Previous studies have shown that the SMMR or SSM/I ice concentration isopleth which best corresponds to the ice edge can be anywhere from 10% to 50% [*Cavalieri*, 1992].

The discrepancies as to which SMMR or SSM/I ice concentration isopleth best defines the ice edge are most likely due to ice concentration retrieval errors associated with different temperature and wind regimes in the MIZ which were not mitigated by the weather filter. In addition, time differences in acquisition of validation data can contribute to discrepancies. For example, in this study the AVHRR image is from one pass, whereas the SSM/I image is the mean of several passes for that day. Since the ice edge is highly diffuse, it is more susceptible to wind and oceanic forcing and could change position and concentration on time scales of hours. Other sources of error could be (1) the use of hemispheric tie-points which ignores variations in brightness temperature, observed particularly along ice edges and in diffuse ice areas, and (2) the under sampling by the 37 GHz frequency of large brightness temperature contrasts associated with marginal ice zones [*Steffen and Schweiger*, 1990]. These errors also contribute to differences in *total* ice concentration estimates between images from one day to the next or between two different satellite images of the same day.

One of the objectives of this study was to see how NASA Team SSM/I derived ice concentrations compare to AVHRR derived ice concentrations for an Antarctic MIZ and coastal area, two features which are predominant in the LTER study area. According to the October 10 comparison (which is lesser problematic than the September 30 comparison), SSM/I derived ice concentrations on average overestimate surface ice concentrations when considering the entire scene, which includes a highly diffuse MIZ and open and close pack ice. However, it is informative to separate these areas to see how the SSM/I and AVHRR derived ice concentrations compare for each of these ice regimes. Based on the October 10 comparison, SSM/I derived ice concentrations (1) overestimate in the MIZ (AVHRR values between 0-40%) by 17.4% ±17.8%, (2) overestimate in open pack areas (AVHRR values between 40-75%) by 10.8% ±11.3%, and (3) underestimate in close pack areas (AVHRR values between 75-100%) by 9.2% ±6.9%. It is clear, however, that more comparisons of SSM/I and AVHRR derived ice concentrations are needed of areas with varying sea ice concentrations from 0 to 100% in order to confirm whether the above results are the general case for the western Antarctic Peninsula region.

Qualitatively, the high resolution AVHRR imagery show some significant features such as leads, polynyas and diffuse marginal ice zones, which are not apparent in the lower resolution SSM/I imagery, but which have important physical and biological implications in polar regions. Heat and mass balance fluxes between ocean and atmosphere in polar regions are strongly influenced by openings in pack ice and by formation of new ice in these openings and in marginal ice zones [*Maykut*, 1982; *Maykut*, 1986]. In addition, the greater the fraction of open water, the more photosynthetically available radiant energy (PAR) entering the water column for support of photosynthesis, both within the water column and under nearby sea ice. However, the greater the fraction of open water, especially in spring, the greater the exposure of surface waters to UV radiation and wind mixing of the euphotic zone, factors which can reduce primary production and hence the well-being of secondary consumers. Leads, polynyas and diffuse marginal ice zones also have other important implications for marine communities, which either benefit from open water or pack ice as a habitat and/or as a source of high concentrations of food. The two springtime AVHRR images of the western Antarctic Peninsula analyzed here show that these ecologically important features can be prominent in the LTER region and will need to be considered, in addition to total estimates of ice coverage provided by the passive microwave data, when assessing ice-ecosystem relationships.

6.3. LTER Ice-Ecosystem Dynamics

The key hypothesis of the Palmer LTER program, which states that interannual and annual variability in sea ice coverage is the major determinant in spatial and temporal changes in Antarctic marine communities, is supported by many studies. For example, phytoplankton blooms have been observed both in the vicinity of retreating ice edges in spring [*Smith and Nelson*, 1985; *Wilson et al.*, 1986; *Nelson et al.*, 1987; *Sullivan et al.*, 1988; *Smith and Nelson*, 1990; *Comiso et al.*, 1993] and along stationary ice edges in summer and winter [*Dieckmann*, 1987; *Nelson et al.*, 1989; *Comiso et al.*, 1990], and it is believed that ice-edge blooms contribute significantly to the total production of the Southern Ocean [*Smith and Nelson*, 1986; *Smith et al.*, 1988]. In addition, the contribution from sea ice algal and bacterial production on total productivity appears to be significant as well [*Grossi et al.*, 1987; *Kottmeier and Sullivan*, 1987; *Kottmeier et al.*, 1987; *SooHoo et al.*, 1987; *Garrison*, 1991]. Krill, a primary consumer, comprise over 50% of the total zooplankton biomass in the Southern Ocean epipelagic layer and therefore represent half the biomass for consumption by larger carnivores [*Hopkins*, 1985; *Laws*, 1985]. Krill have been observed to be concentrated along the ice edge in spring and under the ice in winter, presumably grazing on ice edge blooms and sea ice algae [*Kottmeier and Sullivan*, 1987; *Garrison and Buck*, 1989; *Smetacek et al.*, 1990; *Ross and Quetin*, 1991]. Secondary consumers such as Adélie penguins not only depend on krill for food [*Trivelpiece et al.*, 1987] but are dependent both on pack ice for winter survival and on access to open water near breeding colonies in spring [*Ainley et al.*, 1983; *Ainley et al.*, 1988; *Fraser et al.*, 1992]. Thus, the spatial and temporal variability in sea ice effects both Adélie recruitment and population growth. *Hunt* [1991] discusses the influence of sea ice coverage on seabird environments and points out that trophic level coupling varies both in space and time. He describes three *different* springtime seabird habitats associated with sea ice coverage which therefore have different implications on trophic level coupling: (1) open leads and polynyas, through which seabirds can gain access to the water column and underside of sea ice, (2) the ice edge, which can either be compact or highly diffuse, and which is a major ecological boundary, and (3) the *outer* marginal ice zone, where meltwater contributes to stabilization of the water column. These observations indicate that interannual variability in sea ice coverage, and type of ice coverage, impact, both directly and indirectly, interannual variability at all trophic levels of the Antarctic food web.

In short, passive microwave data have provided regional scale information on the spatial and temporal variability of sea ice within the LTER region. This region is distinguished by an annual cycle showing a relatively short period of ice advance (about 5 months) followed by a longer period of ice retreat (7 months) and a long term persistence, wherein two to four high ice years are followed by one to three low ice years. This oscillation of high and low ice years has been shown to be linked to ENSO [*Smith et al.*, this volume]. It is also a region influenced by a large proportion of MIZ and open pack ice areas and numerous leads and polynyas that require higher resolution satellite imagery for detection and assessment. In addition, higher resolution satellite data is needed in order to understand and establish ice-ecosystem linkages within the sea bird foraging area of Anvers Island. Towards this objective, analysis of visible and infrared imagery, when cloud-free conditions exists, will continue, and it is hoped that Synthetic Aperature Radar (SAR) data will be available for more intensive high resolution analyses.

Acknowledgments. This work was funded by NSF grant DPP90-11927. The National Snow and Ice Data Center (Boulder, Colorado) made available the SMMR and SSM/I sea ice concentration data, and we would like to thank in particular Michelle Holm for her many efforts and support at NSIDC. We would also like to thank Bob Whritner and Beth Sharp at the Arctic and Antarctic Research Center (San Diego, California), who made available the AVHRR data. The analysis of cloud-free AVHRR imagery was made possible by Andy Archer who screened the 350 mostly cloudy AVHRR images. Computing resources were provided by the Institute for Computational Earth System Science. Finally, we would like to thank Karen Baker, Joel Michaelson, Dave Siegel, Libe Washburn and two reviewers for their critical comments and useful suggestions. This is Palmer LTER contribution #80.

REFERENCES

Ackley, S. F., Mass-balance aspects of Weddell Sea pack ice, *Journal of Glaciology*, *24*(90), 391-405, 1979.

Ainley, D. G., R. E. LeResche, and W. J. L. Sladen, *Breeding Biology of the Adelie Penguin*, Berkely, CA, University of California Press, 240 pp, 1983.

Ainley, D. G., W. R. Fraser, C. W. Sullivan, J. J. Torres, T. L. Hopkins, and W. O. Smith, Antarctic mesopelagic micronekton: evidence from seabirds that pack ice affects community structure, *Science*, *232*, 847-849, 1986.

Ainley, D. G., W. R. Fraser, and K. L. Daly, Effects of pack ice on the composition of micronektonic communities in the Weddell Sea, in *Antarctic Ocean and Resources Variability*, edited by Sahrhage, D., pp. 140-146, Springer-Verlag, Berlin-Heidelberg, 1988.

Allison, I., R. E. Brandt, and S. G. Warren, East Antarctic sea ice: albedo, thickness distribution, and snow cover, *J. Geophys. Res.*, *98*, 12417-12429, 1993.

Budd, W. F., The role of Antarctica in Southern Hemisphere weather and climate, *Australian Meteorological Magazine*, *30*(4), 265-272, 1982.

Carleton, A. M., Ice-ocean-atmosphere interactions at high southern latitudes in winter from satellite observation, *Australian Meteorological Magazine*, *29*, 183-195, 1981.

Carleton, A. M., and D. A. Carpenter, Intermediate-scale sea ice-atmosphere interactions over high southern latitudes in winter, *Geo Journal*, *18*(1), 87-101, 1989.

Cavalieri, D. J., The validation of geophysical products using multisensor data, in *Microwave Remote Sensing of Sea Ice*, edited by Carsey, F. D., pp. 233-242, American Geophysical Union, Washington, D.C., 1992.

Cavalieri, D. J., and C. L. Parkinson, Large-scale variations in observed Antarctic sea ice extent and associated atmospheric circulation, *Monthly Weather Review*, *109*(11), 2323-2336, 1981.

Cavalieri, D. J., and H. J. Zwally, Satellite observations of sea ice, *Adv. Space Res.*, *5*(6), 247-255, 1985.

Cavalieri, D. J., W. J. Campbell, and P. Gloersen, Determination of sea ice parameters with the NIMBUS 7 SMMR, *J. Geophys. Res.*, *89*(D4), 5355-5369, 1984.

Cavalieri, D. J., M. R. Drinkwater, D. T. Eppler, L. D. Farmer, R. R. Jentz, and C. C. Wackerman, Aircraft active and passive microwave validation of sea ice concentration from the Defense Meteorological Satellite Program Special Sensor Microwave Imager, *J. Geophys. Res.*, *96*(C12), 21989-22008, 1991.

Cavalieri, D. F., K. M. St. Germain, and C. T. Swift, Reduction of weather effects in the calculation of sea ice concentration with the DMSP SSM/I, in press, *J. Glaciol.* 1995.

Chapman, W. L., and J. E. Walsh, Recent variations of sea ice and air temperature in high latitudes, *Bulletin American Meteorological Society*, *74*(1), 33-47, 1993.

Comiso, J. C., Sea ice effective microwave emissivities from satellite passive microwave and infrared observations, *J. Geophys. Res.*, *88*(C12), 7686-7704, 1983.

Comiso, J. C., and S. F. Ackley, Antarctic sea ice passive microwave signatures during summer and autumn, *IEEE*, *1*, 143-146, 1994.

Comiso, J. C., and H. J. Zwally, Antarctic sea ice concentrations inferred from Nimbus 5 ESMR and Landsat Imagery, *J. Geophys. Res.*, *87*(C8), 5836-5844, 1982.

Comiso, J. C., S. F. Ackley, and A. L. Gordon, Antarctic sea ice microwave signatures and their correlation with in situ ice observations, *J. Geophys. Res.*, *89*(C1), 662-672, 1984.

Comiso, J. C., W. O. Smith, C. W. Sullivan, and N. G. Maynard, Satellite ocean color studies of Antarctic ice edges in summer and autumn, *J. Geophys. Res.*, *95*(C6), 9481-9496, 1990.

Comiso, J. C., T. C. Grenfell, M. Lange, A. W. Lohanick, R. K. Moore, and P. Wadhams, Microwave remote sensing of the Southern Ocean ice cover, in *Microwave Remote Sensing of Sea Ice*, edited by Carsey, F. D., pp. 243-259, American Geophysical Union, Washington, D.C., 1992.

Comiso, J. C., C. R. McClain, C. W. Sullivan, J. P. Ryan, and C. L. Leonard, Coastal Zone Color Scanner pigment concentrations in the Southern Ocean and relationships to geophysical surface features, *J. Geophys. Res.*, *98*, 2419-2451, 1993.

Dieckmann, G., High phytoplankton biomass at the advancing ice edge in the northern Weddell Sea during winter, *EOS Trans.*, *68*, 1765, 1987.

Emery, W. J., M. Radebaugh, C. W. Fowler, D. J. Cavalieri, and K. Steffen, A comparison of sea ice parameters computed from Advanced Very High Resolution Radiometer and Landsat satellite imagery and from airborne passive microwave radiometry, *J. Geophys. Res.*, *96*, 22,075-22,085, 1991.

Emery, W. J., C. Fowler, and J. Maslanik, Arctic sea ice concentrations from Special Sensor Microwave Imager and Advanced Very High Resolution Radiometer satellite data, *J. Geophys. Res.*, *99*, 18,329-18,342, 1994.

Fraser, W. R., and D. G. Ainley, Ice edges and seabird occurrence in Antarctica, *BioScience*, *36*, 258-263, 1986.

Fraser, W. R., W. Z. Trivelpiece, D. G. Ainley, and S. G. Trivelpiece, Increases in Antarctic penguin populations: reduced competition with whales or a loss of sea ice due to environmental warming? *Polar Biology*, *11*, 525-531, 1992. Palmer LTER Contribution #35.

Garrison, D. L., Antarctic sea ice biota, *American Zool.*, *31*, 17-33, 1991.

Garrison, D. L., and K. R. Buck, The biota of Antarctic pack ice in the Weddell Sea and Antarctic Peninsula regions, *Polar Biol.*, *10*, 211-219, 1989.

Garrison, D. L., K. R. Buck, and G. A. Fryxell, Algal assemblages in Antarctic pack ice and in ice-edge plankton, *J. Phycol.*, *23*, 564-572, 1987.

Gloersen, P., and F. T. Barath, Scanning Multichannel Microwave Radiometer for Nimbus-G and Seasat-A, *IEEE Journal of Ocean Engineering*, *OE-2*, 172-178, 1977.

Gloersen, P., and D. J. Cavalieri, Reduction of weather effects in the calculation of sea ice concentrations from microwave radiances, *J. Geophys. Res.*, *91*, 3913-3919, 1986.

Gloersen, P., W. J. Campbell, D. J. Cavalieri, J. C. Comiso, C. L. Parkinson, and H. J. Zwally, *Arctic and Antarctic Sea Ice, 1978-1987: Satellite Passive-Microwave Observations and Analysis*, 290 pp., National Aeronautics and Space Administration, Washington, D.C., 1992. NASA SP-511.

Gordon, A. L., Seasonality of Southern Ocean sea ice, *J. Geophys. Res.*, *86*(C5), 4193-4197, 1981.

Gordon, A. L., and H. W. Taylor, Seasonal change of Antarctic sea ice cover, *Science*, *187*, 346-347, 1975.

Gow, A. J., S. F. Ackley, W. F. Weeks, and J. W. Govoni, Physical and structural characteristics of Antarctic sea ice, *Ann. Glaciol*, *3*, 113-117, 1982.

Grenfell, T. C., and G. A. Maykut, The optical properties of ice and snow in the Arctic basin, *J. Glaciol.*, *18*(80), 445-463, 1977.

Grossi, S. M., S. T. Kottmeier, R. L. Moe, G. T. Taylor, and C. W. Sullivan, Sea ice microbial communities. VI. Growth and primary production in bottom ice under graded snow cover, *Mar. Ecol. Prog. Ser.*, *35*, 153-164, 1987.

Harangozo, S. A., *Interannual atmospheric circulation-sea ice extent relationships in the Southern Ocean: an analysis for the west Antarctic Peninsula region*, (AMS 6th conference on climate variations, Nashville, Tennessee), 1994.

Hibler, W. D., and S. F. Ackley, Numerical simulation of the Weddell Sea pack ice, *J. Geophys. Res.*, *88*(C5), 2873-2887, 1983.

Hofmann, E. E., J. M. Klinck, C. M. Lascara, and D. Smith, Water Mass Distributions and Circulation West of the Antarctic Peninsula and Including the Bransfield Strait. this volume.

Hollinger, J. P., J. L. Peirce, and G. A. Poe, SSM/I instrument evaluation, *IEEE Transactions on Geoscience and Remote Sensing*, *28*(5), 781-790, 1990.

Hopkins, T. L., Food web of an Antarctic midwater ecosystem, *Marine Biology*, *89*, 197-212, 1985.

Hunt, G. L., Marine birds and ice-influenced environments of polar oceans, *Journal of Marine Systems*, *2*, 233-240, 1991.

Jacobs, S. S., and J. C. Comiso, A recent sea-ice-retreat west of the Antarctic Peninsula, *Geophysical Research Letters*, *20*(12), 1171-1174, 1993.

Jeffries, M. O., K. Morris, A. P. Worby, and W. F. Weeks, Late winter sea-ice properties and growth processes in the Bellingshausen and Amundsen Seas, *Antarct. J. U. S.*, *29*(1), 11-13, 1994a.

Jeffries, M. O., R. A. Shaw, K. Morris, A. L. Veazey, and H. R. Krouse, Crystal structure, stable isotopes (δ^{18} O), and development of sea ice in the Ross, Amundsen, and Bellingshausen seas, Antarctica, *J. Geophys. Res.*, *99*(C1), 985-995, 1994b.

Key, J., and R. G. Barry, Cloud cover analysis with Arctic AVHRR data. 1. Cloud detection, *J. Geophys. Res.*, *94*(D15), 18521-18535, 1989.

Kidwell, K. B., *NOAA Polar Orbiter Data Users' Guide*, NOAA National Satellite Data and Information Services, Washington, D.C., 1991.

Kottmeier, S. T., and C. W. Sullivan, Late winter primary production and bacterial production in sea ice and seawater west of the Antarctic Peninsula, *Mar. Ecol. Prog. Ser.*, *36*, 287-298, 1987.

Kottmeier, S. T., S. M. Grossi, and C. W. Sullivan, Sea ice microbial communities. VIII. Bacterial production in annual sea ice of McMurdo Sound, Antarctica, *Mar. Ecol. Prog. Ser.*, *35*, 175-186, 1987.

Lauritson, L., G. J. Nelson, and F. W. Porto, Data extraction and calibration of Tiros-N/NOAA Radiometers, *NOAA Technical memorandum, NESS 107 (Rev. 1)*, US Department of Commerce, NOAA, National Environmental Satellite, Data and Information Service, 1988.

Laws, R. M., The ecology of the Southern Ocean, *Am. Sci.*, *73*(1), 26-40, 1985.

Manabe, S., R. J. Stouffer, M. J. Spelman, and K. Bryan, Transient responses of a coupled ocean atmosphere model to gradual changes of atmospheric CO_2. 1. Annual mean response, *Journal of Climate*, *4* (8), 785-818, 1991.

Manabe, S., M. J. Spelman, and R. J. Stouffer, Transient responses of a coupled ocean atmosphere model to gradual changes of atmospheric CO_2. 2. Seasonal response, *Journal of Climate*, *5* (2), 105-126, 1992.

Martin, S., B. Holt, D. J. Cavalieri, and V. Squire, Shuttle Image Radar B (SIR-B) Weddell sea ice observations: a comparison of SIR-B and Scanning Multichannel Microwave Radiometer ice concentrations, *J. Geophys. Res.*, *92*(C7), 7137-7179, 1987.

Massom, R., and J. C. Comiso, The classification of Arctic sea ice types and the determination of surface temperature using Advanced Very High Resolution Radiometer data, *J. Geophys. Res.*, *99*, 5101-5218, 1994.

Maykut, G., Large-scale heat exchange and ice production in the central Arctic, *J. Geophys. Res.*, *87*, 7971-7984, 1982.

Maykut, G. A., The surface heat and mass balance, in *The Geophysics of Sea Ice*, edited by Untersteiner, N., (*NATO ASI series. Series B, Physics; v. 146*), pp. 395-463, Plenum Press, New York, 1986.

Mitchell, J. F. B., The "greenhouse" effect and climate change, *Reviews of Geophysics*, *27*, 115-139, 1989.

Nelson, D. M., W. O. Smith, L. I. Gordon, and B. A. Huber, Spring distributions of density, nutrients, and phytoplankton biomass in the ice edge zone of the Weddell-Scotia sea, *J. Geophys. Res.*, *92*(C7), 7181-7190, 1987.

Nelson, D. M., W. O. Smith, R. D. Muench, L. I. Gordon, C. W. Sullivan, and D. M. Husby, Particulate matter and nutrient distributions in the ice-edge zone of the Weddell Sea: relationship to hydrography during late summer, *Deep-Sea Res.*, *36*(2), 191-209, 1989.

Parkinson, C. L., and D. J. Cavalieri, Interannual sea-ice variations and sea-ice/atmosphere interactions in the Southern Ocean, 1973-1975, *Annals of Glaciology*, *3*, 249-254, 1982.

Pease, C. B., AVHRR, in *Satellite Imaging Instruments: Principles, Technologies, and Operational Systems*, edited by Pease, C. B., pp. 176-200, Ellis Harwood, New York, 1991.

Quetin, L. B., and R. M. Ross, A long-term ecological research strategy for polar environmental research, *Marine Pollution Bulletin*, *25*, 233-238, 1992.

Ross, R. M., and L. B. Quetin, Ecological physiology of larval euphausiids, Euphausia superba (Euphausiacea), *Memoirs of the Queensland Museum*, *31*, 321-333, 1991.

Ross, R. M., and L. B. Quetin, Palmer Long-Term Ecological Research (LTER): an overview of the 1991-1992 season, *Antarct. J. U. S.*, *27*(5), 235-236, 1992.

Schwerdtfeger, W., The effect of the Antarctic Peninsula on the temperature regime of the Weddell Sea, *Monthly Weather Review*, *103*(1), 45-51, 1975.

Schwerdtfeger, W., *Weather and Climate of the Antarctic*, (*Developments in Atmospheric Science, 15*), 261 pp., Elsevier Science Pub. Co., New York, 1984.

Smetacek, V., R. Scharek, and E. M. Nothig, Seasonal and regional variation in the pelagial and its relationship to the life history cycle of krill, in *Antarctic Ecosystems: Ecological change & conservation*, edited by Kerry, K. R., and G. Hempel, pp. 103-114, Springer-Verlag, 1990.

Smith, W. O., and D. M. Nelson, Phytoplankton bloom produced by a receding ice edge in the Ross Sea: spatial coherence with the density field, *Science*, *227*, 163-166, 1985.

Smith, W. O., and D. M. Nelson, Importance of ice edge phytoplankton production in the Southern Ocean, *BioScience*, *36*(4), 251-257, 1986.

Smith, W. O., and D. M. Nelson, Phytoplankton growth and new production in the Weddell Sea marginal ice zone in the austral spring and autumn, *Limnol. Oceanogr.*, *35*(4), 809-821. 1990.

Smith, S. J., and J. Vidal, Variations in the distribution, abundance, and development of copepods in the southeastern Bering Sea in 1980 and 1981, *Contint. Shelf Res.*, *5*, 215-239, 1986.

Smith, W. O., N. K. Keene, and J. C. Comiso, Interannual variability in estimated primary production of the Antarctic marginal ice zone, in *Antarctic Ocean and Resources Variability*, edited by Sahrhage, D., pp. 131-139, Springer-Verlag, Berlin, 1988.

Smith, R. C., et al., The Palmer LTER: A long-term ecological research program at Palmer Station, Antarctica, in press, *Oceanography*, 1995.

Smith, R. C., S. Stammerjohn, and K. S. Baker, Surface Air Temperature Variations in the Western Antarctic Peninsula Region, this volume.

SooHoo, J. B., A. C. Palmisano, S. T. Kottmeier, M. P. Lizotte, S. L. SooHoo, and C. W. Sullivan, Spectral light absorption and quantum yield of photosynthesis in sea ice microalgae and a bloom of *Phaeocystis pouchetii* from McMurdo Sound, Antarctica, *Mar. Ecol. Prog. Ser.*, *39*, 175-189, 1987.

Stammerjohn, S. E., *Spatial and temporal variability in Southern Ocean sea ice coverage*, M.S. Thesis, 111 pp., University of California, Santa Barbara, 1993.

Steffen, K., and A. J. Schweiger, A multisensor approach to sea ice

classification for the validation of DMSP-SSM/I passive microwave derived sea ice products, *Photogramm. Eng. Remote Sens.*, *56*, 75-82, 1990.

Steffen, K., and A. Schweiger, NASA team algorithm for sea ice concentration retrieval from Defense Meteorological Satellite Program Special Sensor Microwave Imager: comparison with Landsat satellite imagery, *J. Geophys. Res.*, *96*(C12), 21,971-21,987, 1991.

Steffen, K., J. Key, D. J. Cavalieri, J. Comiso, P. Gloersen, K. M. St. Germain, and I. Rubinstein, The estimation of geophysical parameters using passive microwave algorithms, in *Microwave Remote Sensing of Sea Ice*, edited by Carsey, F. D., pp. 201-231, American Geophysical Union, Washington, D.C., 1992.

Steffen, K. R., et al., Snow and ice applications of AVHRR in polar regions, *Ann. Glaciol.*, *17*, 1-16, 1993.

Streten, N. A., and D. J. Pike, Characteristics of the broadscale Antarctic sea ice extent and the associated atmospheric circulation 1972-1977, *Arch. Met. Geoph. Biokl., Ser. A*, *29*, 279-299, 1980.

Sullivan, C. W., C. R. McClain, J. C. Comiso, and W. O. Smith, Phytoplankton standing crops within an Antarctic ice edge assessed by satellite remote sensing, *J. Geophys. Res.*, *93*(C10), 12487-12498, 1988.

Trivelpiece, W. Z., S. G. Trivelpiece, and N. J. Volkman, Ecological segregation of Adelie, Gentoo, and Chinstrap penguins at King George Island, Antarctica, *Ecology*, *68*, 351-361, 1987.

Walsh, J. J., and C. P. McRoy, Ecosystem analysis in the southeastern Bering Sea, *Contint. Shelf Res.*, *5*, 259-288, 1986.

Wilson, D. L., W. O. Smith, and D. M. Nelson, Phytoplankton bloom dynamics of the Western Ross Sea ice edge - I. Primary productivity and species-specific production, *Deep-Sea Res.*, *33*(10), 1375-1387, 1986.

Zibordi, G., and M. L. Van Woert, Antarctic sea ice mapping using the AVHRR, *Remote Sensing of Environment*, *45*, 155-163, 1993.

Zwally, H. J., J. C. Comiso, C. L. Parkinson, W. J. Campbell, F. D. Carsey, and P. Gloersen, *Antarctic sea ice, 1973-1976: Satellite Passive-Microwave Observations*, 206 pp., NASA SP-459, National Aeronautics and Space Administration, Washington, D.C., 1983.

Sharon Stammerjohn and Raymond C. Smith, Institute for Computational Earth System Science (ICESS), Geography Department, University of California, Santa Barbara, 6812 Ellison Hall, Santa Barbara, CA 93106

(Received December 19, 1994;
Accepted September 18, 1995.)